Calhoun: The NPS Institutional Archive

DSpace Repository

Theses and Dissertations | 1. Thesis and Dissertation Collection, all items

1971

Design and study of a novel fluidic angular rate sensing system.

Patterson, James Wheeler.

Massachusetts Institute of Technology

http://hdl.handle.net/10945/15654

Downloaded from NPS Archive: Calhoun

http://www.nps.edu/library

Calhoun is the Naval Postgraduate School's public access digital repository for research materials and institutional publications created by the NPS community. Calhoun is named for Professor of Mathematics Guy K. Calhoun, NPS's first appointed -- and published -- scholarly author.

Dudley Knox Library / Naval Postgraduate School
411 Dyer Road / 1 University Circle
Monterey, California USA 93943

DESIGN AND STUDY OF A NOVEL FLUIDIC ANGULAR RATE SENSING SYSTEM

James Wheeler Patterson

DESIGN AND STUDY OF A NOVEL FLUIDIC ANGULAR RATE SENSING SYSTEM

by

JAMES WHEELER PATTERSON

B.S., Purdue University
(1965)

Submitted in partial fulfillment of the requirements for the Degree of Master of Science in Mechanical Engineering and the Degree of Master of Science in Naval Architecture and Marine Engineering

at the

Massachusetts Institute of Technology

May 1971

Thesis
P2657

LIBRARY
NAVAL POSTGRADUATE SCHOOL
MONTEREY, CALIF. 93940

DESIGN AND STUDY OF A NOVEL FLUIDIC ANGULAR RATE SENSING SYSTEM

BY

JAMES WHEELER PATTERSON

Submitted to the Departments of Mechanical Engineering and Naval Architecture and Marine Engineering on May 14, 1971, in partial fulfillment of the requirements for the Degree of Master of Science in Mechanical Engineering and the Degree of Master of Science in Naval Architecture and Marine Engineering.

ABSTRACT

An analytical and experimental investigation of the angular rate sensing properties of a fluidic device is presented in three parts. The first part introduces the elements of the fluidic device, and describes and develops the interrelationship of the jet, the emitter, and the receiver ports. Geometrical and parameter constraints are developed and form the foundation for design in Part Two.

The second part of the investigation develops the relationship of angular rotation of the jet to jet deflection, and the relationship of jet deflection to differential output pressure. The design constraints developed in Part One are integrated with the analysis of differential output pressure as a function of angular rotation rate, and the design of the experimental apparatus is completed. Predicted behavior of the angular rotation rate sensor is calculated, and an experimental procedure is formulated.

In Part Three the experimental procedure and results are presented and compared to the predicted behavior of the system. The differential output pressure is found to be proportional to angular rotation rate in a specified range of operation, and to correlate with the predicted behavior of the system. The phenomena of reduction of transition zone length with jet rotation and random instability of the jet, at some reynolds numbers, is observed, and the relationship of reynolds number of the jet and nozzle to receiver port distance to the peak recovery pressure and to the angular rotation rate range are determined.

Thesis Supervisor: S. Y. Lee
Title: Professor of Mechanical Engineering

Thesis Reader: A. D. Carmichael
Title: Professor of Naval Architecture and Marine Engineering

ACKNOWLEDGMENTS

The author wishes to especially thank his thesis supervisors, Professor S. Y. Lee and Professor A. D. Carmichael for their encouragement, support, and guidance in the realization of this thesis.

The author would also like to express his appreciation to the United States Navy for its support of his academic program and financial support of this thesis.

TABLE OF CONTENTS

Chapter			Page
I		Introduction	9
II		Design and Analysis of the Experimental Apparatus	11
	2.1	The Jet	11
	2.2	Receiver Port Geometry	13
	2.3	Emitter Tube Geometry	14
	2.4	Vent Effects	15
	2.5	Environmental Effects	16
	2.6	Jet Deflection as a Function of Angular Rotation Rate	16
	2.7	Differential Output Pressure as a Function of Angular Rotation Rate	20
	2.8	Final Design of the Angular Rate Sensing Device	22
III		Experimental Procedure	25
	3.1	Experimental Apparatus	25
	3.2	Instrumentation	25
	3.3	Determination of Differential Output Pressure	26
IV		Discussion of Results	28
V		Conclusions and Recommendations	34
		References	36
		Figures	37

LIST OF FIGURES

Figure		Page
1	Power Jet Velocity Profile	37
2	Power Jet Velocity Profile Representation	38
3	Geometrical Relationships of the Receiver Ports	39
4	Recovery Pressure vs. Angular Rotation Rate L = 24.80 bo, Re = 530	40
5	Recovery Pressure vs. Angular Rotation Rate L = 24.80 bo, Re = 1060	41
6	Recovery Pressure vs. Angular Rotation Rate L = 24.80 bo, Re = 1595	42
7	Recovery Pressure vs. Angular Rotation Rate L = 24.80 bo, Re = 2125	43
8	Recovery Pressure vs. Angular Rotation Rate L = 28.34 bo, Re = 530	44
9	Recovery Pressure vs. Angular Rotation Rate L = 28.34 bo, Re = 1060	45
10	Recovery Pressure vs. Angular Rotation Rate L = 28.34 bo, Re = 1595	46
11	Recovery Pressure vs. Angular Rotation Rate L = 28.34 bo, Re = 2125	47
12	Recovery Pressure vs. Angular Rotation Rate L = 22.02 bo, Re = 2125	48
13	Recovery Pressure vs. Angular Rotation Rate L = 22.02 bo, Re = 530	49
14	Recovery Pressure vs. Angular Rotation Rate L = 22.02 bo, Re = 1060	50
15	Recovery Pressure vs. Angular Rotation Rate L = 22.02 bo, Re = 1595	51
16	Recovery Pressure vs. Angular Rotation Rate L = 31.91 bo, Re = 530	52
17	Recovery Pressure vs. Angular Rotation Rate L = 31.91 bo, Re = 1060	53

18 Recovery Pressure vs. Angular Rotation Rate
L = 31.91 bo, Re = 1595 54

19 Recovery Pressure vs. Angular Rotation Rate
L = 31.91 bo, Re = 2125 55

20 Recovery Pressure vs. Angular Rotation Rate
L = 28.34 bo, Re = 530, 1060, 1595, 2125 56

21 Recovery Pressure vs. Angular Rotation Rate
L = 22.02 bo, 24.80 bo, 28.34 bo, 31.91 bo,
Re = 2125 57

22 Schematic Drawing of the Experimental Apparatus 58

23 Detail Drawing of the Experimental Apparatus 59

24 Photographs of the Experimental Apparatus 60

25 Photographs of the Experimental Apparatus 61

26 Photographs of the Experimental Apparatus 62

27 Photographs of the Experimental Apparatus 63

NOMENCLATURE

b	Width of potential core of jet (in.)
bo	Width of nozzle (in.)
d	Width of receiver port (in.)
e	Distance from inner edge of receiver to centerline of apparatus (in.)
f	Distance from centerline of receiver to port to centerline of apparatus (in.)
h	Power jet centerline displacement from centerline of apparatus at the receiver (in.)
K	Diffusion constant
L	Nozzle to receiver distance (in.)
Le	Emitter tube length (in.)
P	Pressure ($lb./in^2$)
Pa	Atmospheric pressure ($lb./in^2$)
r	Radius (in.)
R	Gas constant (in^2/sec^2 °R)
T	Gas temperature (°R)
V	Jet velocity (ft./sec.)
Vcl	Jet centerline velocity (ft./sec.)
Vo	Jet velocity at the nozzle (ft./sec.)
Vr	Radial velocity (ft./sec.)
Vra	Average radial velocity (ft./sec.)
X	Radial distance from nozzle (in.)
Xo	Transition zone length (in.)
Y	Distance from centerline of jet (in.)
Ye	Effective jet width (in.)

Ymax	Maximum jet width (in.)
ρ	Density of air ($lb./in^3$)
μ	Fluid viscosity ($lb.sec./in^2$)
ω	Angular rotation rate (RPM)
Re	Reynolds number
$V\theta$	Angular velocity (ft./sec.)
$V\theta'$	Relative angular velocity (ft./sec.)

CHAPTER I

Introduction

In the past decade, there have been significant advances in the field of fluidics. The contributions of Simson[7], Bell[10], Brown[6], and many others, have established a broad base of fundamental theoretical support for the design of fluidic devices. In some areas, design can now proceed from a firm theoretical base, and not depend entirely on empirical results or trial and error design techniques that have had to be utilized in the past.

Fluid power control systems have been utilized for many years, however, the important control functions of signal sensing, signal transmission, signal conversion, and other forms of signal processing have frequently been accomplished by electrical or electronic devices[12]. Two major disadvantages of this kind of system are that it requires a variety of fluid-electrical interfaces, and it requires two or more different types of power sources. The system performance and capability is enhanced by the inherent flexibility and environmental insensitivity of the fluid components and suffers from the environmental sensitivity and complexity of the electrical components. A pure fluid system would only require one power source, and would have the advantage of reduced environmental sensitivity. It would be less complex due to the elimination of the fluid-electrical interface components, and offers a potential economic advantage in fabrication costs.

The purpose of this study is to determine the applicability of a pure fluid system for utilization as an angular rate sensor. The fluidic system that was designed could serve as a rate gyro currently used in attitude control systems on missiles and rockets or as a stable reference platform for marine instrumentation applications. The fluid jet would replace the gyroscope as the sensing element with a subsequent reduction in power requirements, weight, and procurement cost. A fluidic device utilizing a subsonic, laminar, submerged jet with a single emitter and two receiver ports to determine differential output pressure was designed and tested. The apparatus was designed to demonstrate parameter interaction, and was configured to obtain visual indication of blocked load differential output pressure. This investigation was constrained to a single degree of freedom system, and evaluated steady state system performance. In Chapter II the analyis of parameter interaction was carried out to determine the geometrical interrelationship of the emitter-receiver groups. Design constraints were then determined, and the final design of the experimental apparatus was developed in the last section. The experimental procedures and instrumentation are discussed in Chapter III, and the experimental results are compared to the predicted system behavior in Chapter IV. Chapter V completes the study with a summary of the significant results and contains recommendations for future work.

CHAPTER II

Design and Analysis of the Experimental Apparatus

2.1 The Jet

Several representations of submerged free jets in the transition from laminar to turbulent flow are present in the literature. Bell[10] has indicated that none of the representations are valid under all boundary conditions. Each representation is applicable only in its domain of definition. Simson[4][7] has modeled the jet into two zones, the transition zone, and the zone of established flow. In the transition zone, the centerline velocity is equal to the original nozzle velocity, Vo, and in the zone of established flow the centerline velocity decreases with distance from the nozzle. A velocity profile of Simson's representation of the jet is shown in Figure 1, and the nomenclature is defined in Figure 2. This representation of the jet will be used in this study. The jet profile is of the form

$$\frac{Vr}{Vcl} = [1 - (\frac{Ye}{KX})^{\frac{7}{4}}]^2 \qquad (2.1)$$

Where Ye is the effective value of Y for the transition zone, and is the actual value of Y for the zone of established flow, as shown in Figure 2.

In the transition zone the jet profile is of the form

$$Vr = Vo[1 - (\frac{Y-b/2}{KX})^{\frac{7}{4}}]^2 \qquad (2.2)$$

and the average radial velocity, Vra, can be determined by integrating equation (2.2) over the jet profile.

$$Vra = \frac{1}{Ymax} \int_0^{Ymax} Vr\, dY = \frac{1}{Ymax} \int_0^{Ymax} Vo[1 - (\frac{Y-b/2}{KX})^{\frac{7}{4}}]^2 dY \tag{2.3}$$

which, after carrying out the indicated integration, is found to be of the form

$$Vra = Vo \frac{(1 + \frac{0.364X}{Xo})}{(1 + \frac{1.756X}{Xo})}, \tag{2.4}$$

where

$$Ye = Y - b/2 \tag{2.5}$$

$$K = 1.378 \frac{bo}{Xo} \tag{2.6}$$

$$Ymax = KX + b/2 \tag{2.7}$$

$$b = 1/2(1 - X/Xo)\ bo \tag{2.8}$$

In the design of the angular rate sensor, the region of operation of the jet will be limited to the transition zone to minimize the effects of turbulent flow on the receiver ports, thus equations (2.2) and (2.4) characterize the assumed radial velocity profile of the jet.

2.2 Receiver Port Geometry

The primary constraint on the design of the receiver ports was to obtain maximum gain and to maintain linearity of the output pressure with respect to deflection of the jet. For the no-flow, blocked load, condition it will be assumed that the kinetic energy associated with the velocity profile can be used to represent the recovery pressure in the receiver port. Using the nomenclature defined in Figure 3, the recovery pressure can be computed by integrating the velocity profile across the receiver port.[4]

$$PII = \frac{\rho V c l^2}{2d} \int_{e-h}^{e+d-h} [1 - (\frac{Y}{Ymax})^{\frac{7}{4}}]^4 dY \qquad (2.9)$$

$$PI = \frac{\rho V c l^2}{2d} \int_{e+h}^{e+d+h} [1 - (\frac{Y}{Ymax})^{\frac{7}{4}}]^4 dY \qquad (2.10)$$

After differentiation with respect to h, the receiver differential pressure gain is given by

$$\frac{\partial (PII-PI)}{\partial h} = 2(\frac{\rho V c l^2}{2\ Ymax})[f(\frac{\partial (PII-PI)}{\partial h})] \qquad (2.11)$$

where

$$f(\frac{\partial (PII-PI)}{\partial h}) = \frac{[1-(e-h/Ymax)^{\frac{7}{4}}]^4 - [1-(e+d-h/Ymax)^{\frac{7}{4}}]^4}{(2\ d/Ymax)}$$

$$+ \frac{[1-(e+h/Ymax)^{\frac{7}{4}}]^4 - [1-(e+d+h/Ymax)^{\frac{7}{4}}]^4}{(2\ d/Ymax)} \qquad (2.12)$$

As indicated in equation (2.11) and equation (2.12), the receiver gain is a function of receiver port separation, e, and receiver port diameter, d, as well as the centerline velocity, Vcl. This result will be used in Section 2.7 in determining the differential output pressure as a function of angular rotation rate.

2.3 Emitter Tube Geometry

Simply stated, the requirements of the emitter tube are as follows:

1. To produce a stable laminar jet at the nozzle.
2. To have a geometrical form conductive to analysis for calculation of pressure loss across the tube.
3. To have dimensional requirements consistant with the dimensions of the experimental apparatus.
4. To be of a form such that the emitter tube could be fabricated from readily available materials.
5. To be dimensioned such that power source requirements are minimized.

After an extensive analysis, literature survey, and experimental program, Bell[10] determined that the above requirements could be met utilizing commercially available stainless steel hypodermic needle stock. For a range of reynolds numbers of 500-3000, and tube diameters of 0.096 in. to 0.027 in., it was determined that the maximum required

length to diameter ratio, Le/bo, was 100, and that satisfactory results could be obtained by inserting the emitter tube into the plenum chamber at least ten nozzle diameters. Further, end preparation can be limited to grinding the tube ends flat and deburring with a drill point.

Using the above results, a nozzle diameter of 0.047 in., #16 hypodermic tubing, was chosen, and a length to diameter ratio of 75 was selected. The pressure loss across the emitter tube was calculated assuming that the downstream pressure remained at atmospheric pressure, that momentum effects can be neglected, and that the pressure loss is due to pressure and friction effects.[11]

$$(Pu^2 - Pa^2) = \frac{64\ Vo\ \mu\ RT\ Le\ \rho a}{bo^2} \qquad (2.13)$$

2.4 Vent Effects

Vent effects on the jet must be considered under two sets of conditions. The first set of conditions is that the nozzle-receiver port interaction region must be fully vented to prevent the development of a differential pressure across the jet,[5] the interaction chamber enclosing the nozzle-receiver ports must be fully vented to maintain the chamber pressure at atmospheric pressure, and finally, the jet must be shielded from environmental air currents.

The second set of conditions are unique to this study. The same restrictions as outlined in the first set of conditions still hold, however when the entire apparatus is rotated, the jet must be shielded from air currents induced by the rotation of the device. These two sets of conditions require that the interaction chamber be sealed. Thus the final design, as shown in Figure 22 through Figure 27, incorperates an extensive venting configuration.

2.5 Environmental Effects

The primary environmental effects to be considered are atmospheric pressure and ambiant temperature. The ambiant air temperature has a direct relationship to the density of the air, and the atmospheric pressure establishes the required plenum pressure to maintain the desired nozzle velocity, Vo. These factors will be utilized in establishing the required plenum pressures during the experimental phase of this study, and will be monitored during each experimental run.

2.6 Jet Deflection as a Function of Angular Rotation Rate

The starting point for the analysis is the Euler equation for inviscid flow in polar coordinates,[1] with the assumptions of steady state conditions, two dimensional flow, and that no pressure gradiants exist across the jet.

For the angular componet of jet velocity

$$\frac{\partial V\theta}{\partial t} + Vr\,\frac{\partial V\theta}{\partial r} + \frac{V\theta}{r}\,\frac{\partial V\theta}{\partial \theta} + \frac{Vr\ V\theta}{r} = 0 \qquad (2.14)$$

and imposing the continuity condition

$$\frac{\partial Vr}{\partial r} + \frac{1}{r}\,\frac{\partial V\theta}{\partial \theta} = 0 \qquad (2.15)$$

In Section 2.1, the radial velocity profile, as well as the average radial velocity were established.

$$Vr = Vo\left[1 - \left(\frac{Ye - b/2}{KX}\right)^{\frac{7}{4}}\right]^2 \qquad (2.2)$$

$$Vra = Vo\,\frac{\left(1 + \frac{0.364X}{Xo}\right)}{\left(1 + \frac{1.756X}{Xo}\right)} \qquad (2.4)$$

The coordinates are now transformed to a moving reference frame rotating at an angular rotation rate ω.

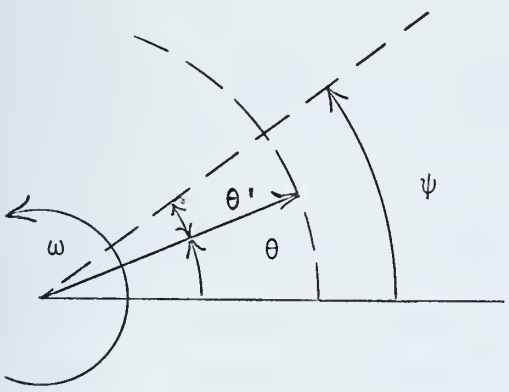

$$\psi = wt$$

$$\theta' = \psi - \theta$$

$$\theta' = wt - \theta$$

$$V\theta' = V\theta - r\omega \qquad (2.16)$$

Where $V\theta'$ is the angular jet velocity relative to the moving coordinate frame, and θ' is the angular displacement of the jet centerline relative to the moving coordinate frame.

Substituting equations 2.16, 2.4, and 2.15 into equation 2.14, the following differential equation for relative angular velocity is obtained.

$$\frac{\partial V\theta'}{\partial r} + V\theta'\left[\frac{1}{r} + \frac{1.392/Xo}{(1 + \frac{1.756r}{Xo})(1 + \frac{0.364r}{Xo})}\right] + 2\omega = 0 \quad (2.17)$$

It was observed that in the range $0.25 \leq \frac{r}{Xo} \leq 0.9$ the coefficient of the $V\theta'$ term can be approximated by $1.30/r$ with less than five percent error. This substitution simplifys the solution considerably, and does not introduce significant error. With this substitution equation 2.17 simplifys to

$$\frac{\partial V\theta'}{\partial r} + \frac{1.30}{r} V\theta' + 2\omega = 0 \quad (2.18)$$

which has as a solution

$$V\theta' = \frac{\text{constant}}{r^{1.3}} - 0.87\omega r \quad (2.19)$$

The solution for the relative angular velocity component has two distinct parts. The first term describes the relative angular velocity component of the flow within the jet. The

constant can be evaluated using the assumed radial velocity profile and continuity and momentum conditions, however this term is not the most significant to this study. The second term is the interesting result. It shows the relationship of the relative angular velocity of the jet centerline to the angular rotation rate of the reference frame. This term of the solution will be used to determine jet deflection as a function of angular rotation rate.

for $V\theta' << Vra$

$$\tan \theta' = \frac{V\theta'}{Vra} \doteq \theta'$$

Thus jet deflection, h, can be calculated directly

$$h = \int_o^L \theta' \, dr = \int_o^L \frac{V\theta'}{Vra} \, dr = \int_o^L \frac{0.87\omega r \, dr}{Vo \frac{(1+\frac{0.364r}{Xo})}{(1+\frac{1.756r}{Xo})}} \qquad (2.20$$

which has as a solution

$$h = \frac{0.87\omega Xo^2}{Vo} \left[18.203(1+\frac{0.364L}{Xo})^2 - 65.266(1+\frac{0.364L}{Xo})\right.$$

$$\left. + 28.859 \log (1+\frac{0.364L}{Xo}) + 47.063\right] \qquad (2.21)$$

This result illustrates several design parameter inter-relationships. The centerline jet deflection is shown to be proportional to angular rotation rate for fixed transition lenght, jet velocity, and nozzle to receiver distance. However, jet deflection is not proportional to jet velocity, transition length, or nozzle to receiver distance for all other parameters held constant.

Bell[10] has shown that the transition length of a submerged jet is a function of reynolds number, thus a change in nozzle velocity also changes the transition length with a resultant non-linear change in jet centerline deflection. The most important result for the design of the apparatus is that for fixed nozzle to receiver distance and nozzle velocity, the jet deflection is proportional to angular rotation rate of the apparatus.

2.7 Differential Output Pressure as a Function of Angular Rotation Rate

The analysis of differential output pressure as a function of angular rotation rate proceeds from the results of Sections 2.1, 2.2, and 2.6, of which the essential results are repeated for continuity.

$$\frac{Vr}{Vcl} = [1 - (\frac{Y}{Ymax})^{\frac{7}{4}}]^2 \qquad (2.1)$$

$$PII = \frac{\rho Vcl^2}{2d} \int_{e-h}^{e+d-h} [1 - (\frac{Y}{Ymax})^{\frac{7}{4}}]^4 dY \qquad (2.9)$$

$$PI = \frac{\rho Vcl^2}{2d} \int_{e+h}^{e+d+h} [1 - (\frac{Y}{Ymax})^{\frac{7}{4}}]^4 dY \qquad (2.10)$$

Simson[4] has evaluated equations 2.9 and 2.10 and defined the following functions

$$C = \frac{Ye}{Ye\ max} = \frac{Y}{Ymax} \qquad (2.22)$$

$$\int_o^Y Vr^2 dY = Vo^2 Ymax[f(C)] \qquad (2.23)$$

where

$$f(C) = [C - \frac{16}{11} C^{\frac{11}{4}} + \frac{28}{18} C^{\frac{18}{4}} - \frac{16}{25} C^{\frac{25}{4}} + \frac{4}{32} C^{\frac{32}{4}}] \qquad (2.24)$$

Substituting the results of equations 2.23 and 2.24 into equations 2.9 and 2.10, the results are obtained

$$\frac{PII}{1/2\ \rho\ Vcl^2} = \frac{f(\frac{e+d-h}{Ymax}) - f(\frac{e-h}{Ymax})}{d/Ymax} \qquad (2.25)$$

$$\frac{PI}{1/2\ \rho\ Vcl^2} = \frac{f(\frac{e+d+h}{Ymax}) - f(\frac{e+h}{Ymax})}{d/Ymax} \qquad (2.26)$$

and by subtracting equation 2.26 from equation 2.25, the normalized differential output pressure is obtained

$$\frac{PII - PI}{1/2\ \rho\ Vcl^2} = \frac{f(\frac{e+d-h}{Ymax}) - f(\frac{e+d+h}{Ymax}) + f(\frac{e+h}{Ymax}) - f(\frac{e-h}{Ymax})}{d/Ymax} \tag{2.27}$$

This result, in conjunction with equations 2.21 and 2.24, will be used in determining the final design, and in the calculation of the predicted behavior of the system.

2.8 Final Design of the Angular Rate Sensing Device

In Sections 2.1 through 2.7 the parameter interrelationships and some design constraints have been established. In this section, the final design of the apparatus will proceed using these relationships and the limitations imposed by facilities and materials that are available.

The maximum angular rotation rate was limited to 100 RPM. This limitation was imposed by the requirement to visually read the water manometers which were designed to be mounted to the apparatus at the axis of rotation. An initial trial indicated that above this rate the manometers could not be interpreted with sufficient clarity.

The emitter tube diameter was established at 0.047 in. This size was selected to limit the length of the emitter tube, to reduce the power source requirements, and to limit the plenum pressure required to establish a nozzle velocity

corresponding to reynolds numbers in the range of 500-3000. An emitter tube length of 75 nozzle diameters was used to produce a stable laminar jet, and the emitter tube was designed to protrude ten nozzle diameters into the plenum chamber.

The range of suitable nozzle to receiver distances was established by the range of reynolds numbers of the jet. A laminar jet was required to avoid the detremental effects of a turbulent flow on the recovery pressure. Bell[10] has shown that for reynolds numbers less than 2000 a transition zone length of greater than 33 nozzle diameters could be established, with corresponding greater transition zone lengths as reynolds number is reduced. An analysis of equation 2.21 indicates that by using the maximum obtainable transition zone length, the jet deflection will be maximized, thus a nozzle to receiver port distance range was established at 20 to 33 nozzle diameters.

The receiver geometry was designed to obtain the maximum gain consistant with linearity. An examination of equations 2.11 and 2.12 indicates that to design for maximum gain would result in unsatisfactory linearity of the output pressure, whereas to design for constant gain would result in unsatisfactory output pressure. A maximum differential output pressure of the order of one inch of water was desired, thus this constraint was used in establishing the dimensions of the receiver ports at a diameter, after deburring, of 0.0425 in. with a port separation of 0.0156 in.

Venting of the interaction chamber was provided by four shielded vent taps of sufficient area to assure constant venting of the chamber and to exclude air currents generated by rotation of the apparatus.

The final dimensions of the experimental apparatus are shown in Figure 22 and Figure 23, and the completed apparatus is shown in Figures 24 through 27.

CHAPTER III

Experimental Procedure

3.1 Experimental Apparatus

The angular rate sensor was directly mounted to a vertical output, geared reduction, 1/70 horsepower bodine model NSA-117 universal motor. The motor was installed on a rubber mounted rigid plate. The air supply was obtained from line pressure reduced to approximately one psig, with final air pressure regulation provided by a needle valve. The air supply was filtered prior to introduction into the apparatus, and was coupled to the apparatus through a locally prepared rotary coupling. Speed control of the motor was provided by a General Radio Co. Type 200-C variable voltage supply with a Dayton Model 4X796 electronic speed control unit installed in series with the motor for final adjustment of motor speed.

All experiments were conducted in a temperature controlled environment with a mean temperature of 77°F prevailing during the course of all experiments. A schematic drawing of the experimental apparatus is shown in Figure 22.

3.2 Instrumentation

Five parameters were to be monitored, plenum pressure, differential output pressure, angular rotation rate, ambiant air temperature, and atmospheric pressure.

Plenum pressure and differential output pressure were measured using water manometers mounted on the experimental apparatus at the axis of rotation. The manometer had a scale graduation of 0.10 inches. All scale readings were taken visually with an estimated error of ±0.01 inches.

Angular rotation rate of the experimental apparatus was measured using a General Radio Co. Type 631-B strobotac electronic tachometer. All measurements were taken using motor speed, and were mathematically converted to angular rotation rate of the experimental apparatus using the fixed gear reduction ratio of 6:1 of the motor drive. The error in angular rotation rate measurement was estimated to be ±0.5 RPM.

Ambiant air temperature was monitored using a direct reading mercury thermometer. The error in temperature readings is estimated at ±0.1°C. Atmospheric pressure was obtained from a local weather data gathering system.

3.3 Determination of Differential Ouput Pressure

The experimental phase of this study was arranged to determine three characteristics of the experimental angular rate sensor. The first, and foremost, goal was to determine the applicability of a fluidic device as an angular rate sensor. The second goal was to experimentally verify the variation in output characteristics with reynolds number of the jet, and finally to experimentally verify the variation

in output characteristics with a change in nozzle to receiver distance. The experiments were divided into four groups corresponding to a range of nozzle to receiver distances of 22 to 32 nozzle diameters. At each nozzle to receiver distance, data was gathered at four reynolds numbers in the range of 500 to 2200.

Each experimental data run was conducted using the same procedure. The plenum pressure was adjusted to the desired pressure, and the receiver ports were centered in the jet in the static, no-rotation, condition using the receiver carrige adjustments to obtain zero output pressure. The apparatus was then brought up to the desired rotational speed, and the resulting differential output pressure and angular rotation rate were recorded. At each data point the plenum pressure was adjusted to the desired value to compensate for the slight variation in the leakage rate at the rotary joint.

CHAPTER IV

Discussion of Results

The general results are presented in two forms. Figures 4 through 19 represent the results of sixteen basic configurations used in the experimental phase, and Figures 20 and 21 present composites of a fixed nozzle to receiver distance with variation in jet reynolds number, and a fixed jet reynolds number with variation in nozzle to receiver distances. All data points have been plotted directly after normalization, and each figure represents a combination of data from two or more experimental runs. No data reduction or averaging techniques were employed, thus the data plotted contains randum experimental error inherent in any data gathering process.

The correlation of the experimental results to the calculated behavior was, in general, quite good with a nominal deviation of the experimental results from the calculated behavior of the order of 25 percent in the nozzle to receiver distance range of 22.02 bo to 28.34 bo with a reynolds number greater than 530. The correlation of the experimental results to the calculated behavior for a reynolds number of 530 was in general quite poor and a wide range of data scattering was evident. The experimental results at a nozzle to receiver distance of 31.91 bo was significantly lower than the calculated behavior by a factor of the order of

100 percent. This result is significant in that the experimental results exceeded the calculated behavior for all other nozzle to receiver distances.

The significant reduction in recovery pressure at the nozzle to receiver distance of 31.91 bo and a jet reynolds number of 1595 and 2125 can potentially be attributed to a transition of the jet to turbulent flow. Bell[10] determined that the transition zone distances corresponding to the reynolds numbers used in this study are as follows:

Reynolds Number	Transition Distance (Nozzle Diameters)
2125	30
1595	42
1060	65 (estimated)
530	75 (estimated)

This data was obtained under circumstances designed to minimize external disturbances, thus it represents the maximum obtainable under ideal conditions. In this study significant disturbances were introduced due to the rotation of the sensor, thus it is very possible that the transition to turbulent flow occurred at a transition distance less then that predicted by Bell with a resultant reduction in recovery pressure. This phenomenon of reduction of transition zone distance with angular rotation will require further study with an experimental apparatus designed to measure the transition zone distance.

The data obtained at a reynolds number of 530 indicates considerable scatter which can be attributed to the experimental error introduced by the resolution limit of the manometer scale. The maximum recovery pressure at this reynolds number was of the order of 0.12 inches of water whereas the minimum scale graduation was 0.10 inches, thus the experimental error inherent in reading the scale was estimated at ±0.02 inches. This data scattering became evident when more than one experimental run was plotted on a single figure. Each run was consistant, within that set of data, but when a second run of data was plotted, the resultant graph exhibited considerable data scattering.

The resultant differential output pressure was observed to be linear up to a value of angular rotation rate corresponding to approximately 80 percent of the angular rotation rate at which the peak output pressure was obtained. This result is consistant with the behavior predicted by equation (2.21) and equation (2.27), and demonstrates the potential suitability of this device as an angular rate sensor. It was further noted that the angular rotation rate at which the peak output pressure was obtained is a function of reynolds number and nozzle to receiver distance, as predicted by equation (2.21), thus the device can be designed for linear operation and maximum output pressure for any desired range of angular rotation rates.

The maximum differential output pressure was observed to become unstable for flows corresponding to reynolds numbers of 1595 and 2125. This phenomenon exhibited itself by the differential output pressure increasing with angular rotation rate until some maximum value was reached, at which time the differential output pressure went into a random oscillation. The random oscillation of the output pressure indicated that the jet was oscillating randomly due to some interaction with the receiver port geometry. This phenomenon of oscillation of a laminar jet as a function of reynolds number has been investigated by Ever.[8] Ever found that, for blocked load conditions, the jet would be stable for reynolds numbers less than 1000, but for reynolds numbers in the range of 1000 to 2500, the jet would interact with the receiver geometry and exhibit random oscillation. For reynolds number greater than 2500, the jet would develop a limit cycle type of oscillation. The oscillation of the jet is detremental to the performance of the device as a sensor, as it limits the angular rotation rate range of the device and the maximum obtainable output pressure. It should be noted from the plotted results that where instability of the jet occurred, a peak in the output pressure was not obtained.

In addition to the assumptions stated in Sections 2.1, 2.6, and 2.7, it should be noted that an additional assumption was made in modeling the jet profile representation. Equation (2.1) includes viscous effects on the submerged jet, thus the

radial velocity profile includes viscous forces. In determining the angular velocity componet and relative angular velocity componet the assumption was made of inviscid flow, thus the resultant relative angular velocity representation, equation (2.19), does not directly include viscous effects. The impact of this assumption on the calculated behavior of the system was estimated to be very small, and in any case less than that introduced by the assumed velocity profile, however, it does potentially contribute the error present in the calculated behavior.

A limited, qualitive, experiment was conducted to determine the interaction of the direction of rotation on the output pressure. It was observed that the sign of the output pressure reversed with a reversal of direction of rotation, and that the magnitude of the resultant output pressure was essentially unchanged, however, this result is somewhat limited in scope due to the lack of sufficient data gathered due to the limitations of the experimental apparatus. The device has symmetrical geometry so that equation (2.21) is still valid and the jet deflection is unchanged except for direction, thus the device is directionally sensitive, and can identify the direction of rotation by the relative magnitude of the blocked load recovery pressure in the receiver ports.

Another limited qualitive experiment was conducted using a receiver port geometry of significantly different form. In this configuration a single receiver port of the same diameter

as the nozzle was mounted and axially aligned with the nozzle. The receiver port was statically aligned with the jet to obtain maximum recovery pressure. The device was then rotated and the reduction in recovery pressure with angular rotation was noted. This configuration does not offer directional sensitivity, however, it does simplify the construction and alignment of the device. The results are inconclusive, in that an extensive analysis was not conducted to predict the system performance, however, it was noted that the jet remained stable, and that the angular rotation rate range was above that of the experimental apparatus, which was of the order of 150 RPM. This configuration could offer significant advantages in the higher angular rotation rate ranges, however, additional study will be required to demonstrate this capability.

CHAPTER V

Conclusions and Recommendations

In the preceding chapters the analysis and design of a fluidic angular rate sensing system has been developed, and the resulting geometrical and parameter interrelationships have been determined. In general, the experimental results have been observed to agree with the predicted behavior, however, some additional parameter limitations have become evident as a result of the experimental phase of the study. The output pressure was found to be a linear function of angular rotation rate, within a predetermined range, and the output pressure was found to be directionally sensitive, in that it would detect and identify the direction of rotation. The applicable range of reynolds numbers of the jet was found to be constrained by two factors, the low magnitude of recovery pressure available for reynolds numbers less than 1000, and the resultant random jet instability for reynolds numbers in the range of 1000 to 2500. The second effect, jet instability, did not prevent the device from performing satisfactorily, however, it did limit the angular rotation rate range to a value somewhat behow that predicted.

The reduction in differential output pressure for nozzle to receiver distances of the order of the predicted transition zone distance indicates a reduction in transition zone length due to the disturbance created by rotation of the apparatus.

This phenomenon requires further study, however, this investigation does indicate that, for nozzle to receiver distances that do not exceed 85 percent of the predicted transition zone length, satisfactory performance will be obtained.

The experimental results indicate that a fluidic angular rate sensor of this type has considerable design flexibility, and that with suitable choices of jet reynolds number, nozzle to receiver distance, and receiver port geometry, the angular rotation rate range and required output pressure signal magnitude can be readily obtained. The experimental device constructed for this study was not designed to minimize size and weight, thus significant size and weight reductions could be imposed on the design of a practical sensor.

Several parameter and environmental interactions will require further study and resolution before this type of fluidic rate sensor could be utilized with fully predictable behavior. The interaction of translation of the sensor as well as off-center rotation and rotation in more than one plane require study, and temperature sensitivity and dynamic response must be determined for compatible integration of this sensor into a control system. The observed phenomenon of apparent reduction in transition zone length with rotation and random jet instability must be fully investigated to determine their origin and to quantify this phenomenon for its interaction to system design.

REFERENCES

1. Sabersky, R.H., and Acosta, A.J., Fluid Flow, MacMillan, New York, 1964.

2. Mager, A., "Generalization of Boundary-Layer Momentum Integral Equations to Three Dimensional Flows, Including those of Rotating System", NACA Report 1067, 1952.

3. Healey, A.J., "Fluidics Notes on Analog Amplifiers and Systems", unpublished class notes for Course 2.171, M.I.T., December 1970.

4. Simson, A.K., "Gain Characteristics of Subsonic, Pressure Controlled, Proportional, Fluid Jet Amplifiers, Journal of Basic Engineering, June 1966.

5. Healey, A.J., "Vent Effects on the Response of a Proportional Fluid Amplifier", Journal of Basic Engineering, March 1968.

6. Brown, F.T., and Humphrey, R.A., "Dynamics of A Proportional Fluidic Amplifier: Part I and II", Journal of Basic Engineering, June 1970.

7. Simson, A.K., "A Theoretical Study of the Design Parameters of Subsonic, Pressure Controlled, Fluid Jet Amplifiers", Ph.D. Thesis, Mechanical Engineering Department, M.I.T., July 1963.

8. Ever, Z., "Mechanisms of Low Frequency Instability and Noise in Fluid Amplifiers", S.M. Thesis, Mechanical Engineering Department, M.I.T., January 1969.

9. Gurski, R.J., "Static and Dynamic Modeling of a Pressure Controlled Subsonic Fluid Jet Modulator", Sc.D. Thesis, Mechanical Engineering Department, M.I.T., May 1965.

10. Bell, Adam, Carr, "An Analytical and Experimental Investigation of the Turbulence Amplifier", Sc.D. Thesis, Mechanical Engineering Department, M.I.T., May 1969.

11. Blackburn, J.F., Reethof, G., and Shearer, J.L., Fluid Power Control, The M.I.T. Press, 1960.

12. Lee, S.Y., "Pure Fluid Amplifying and Logic Elements, Their Application and Future Potential", unpublished notes for a special summer course in Fluid Power Control, M.I.T., July 1966.

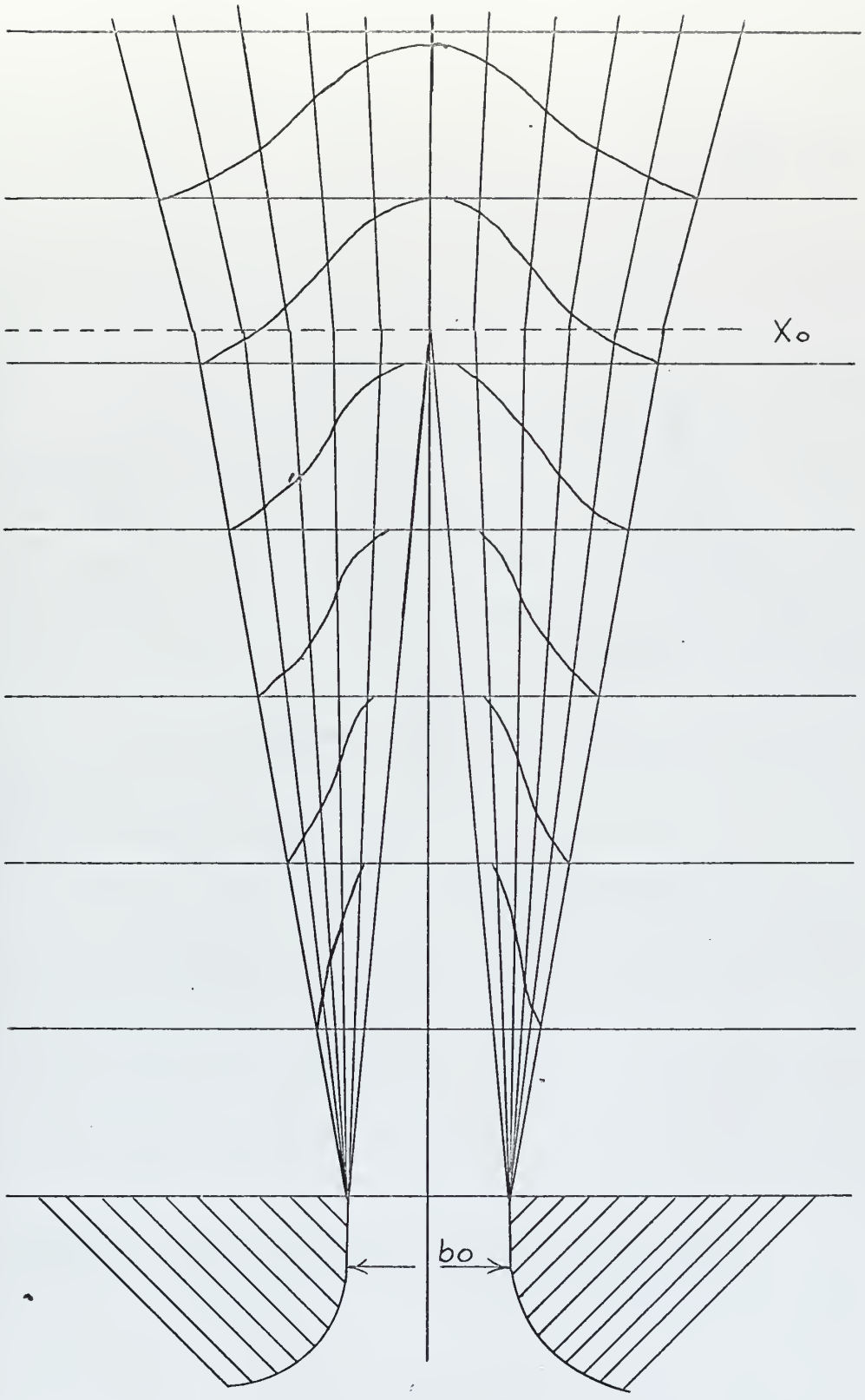

FIGURE 1 POWER JET VELOCITY PROFILE

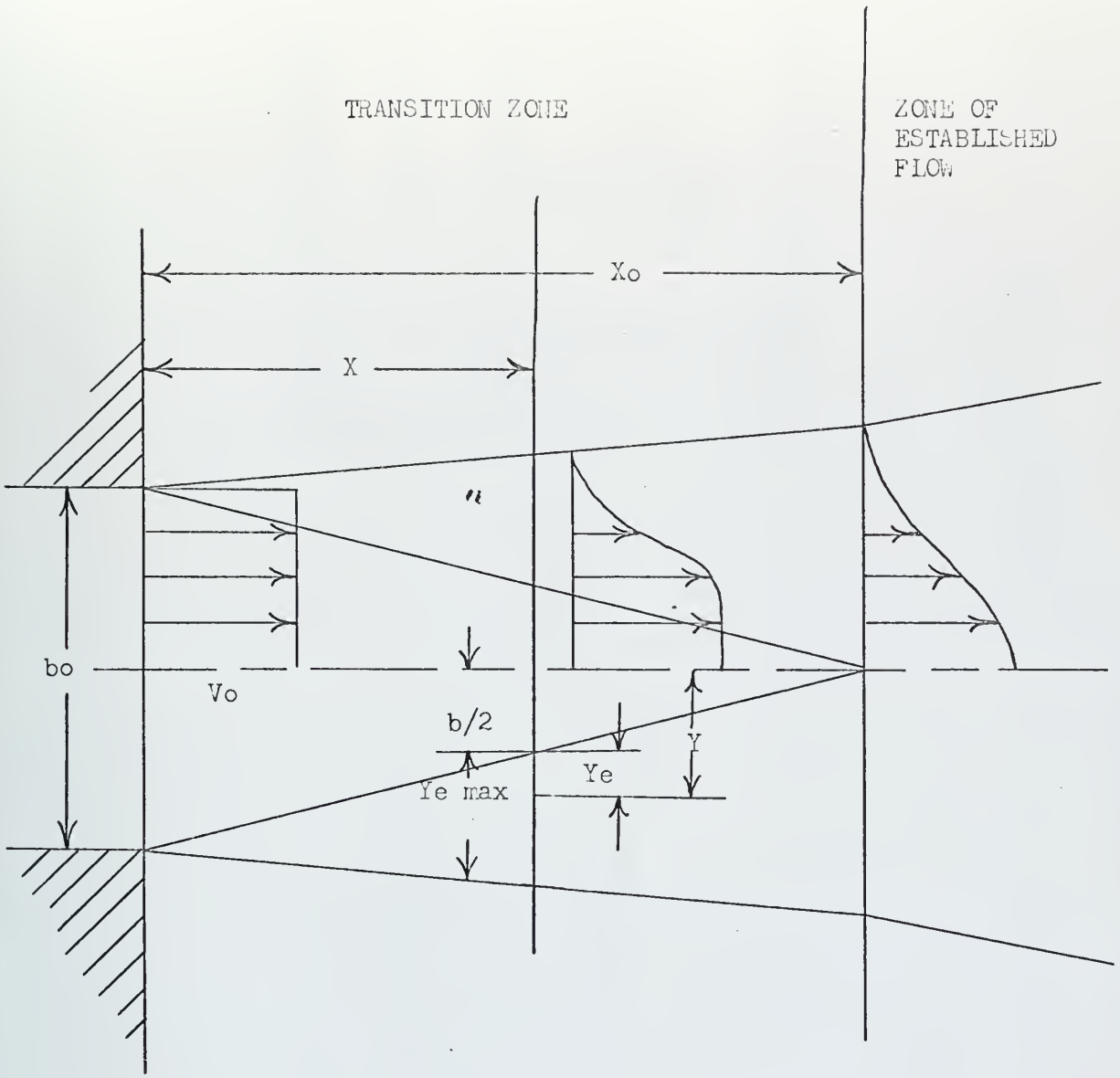

FIGURE 2 POWER JET VELOCITY PROFILE REPRESENTATION

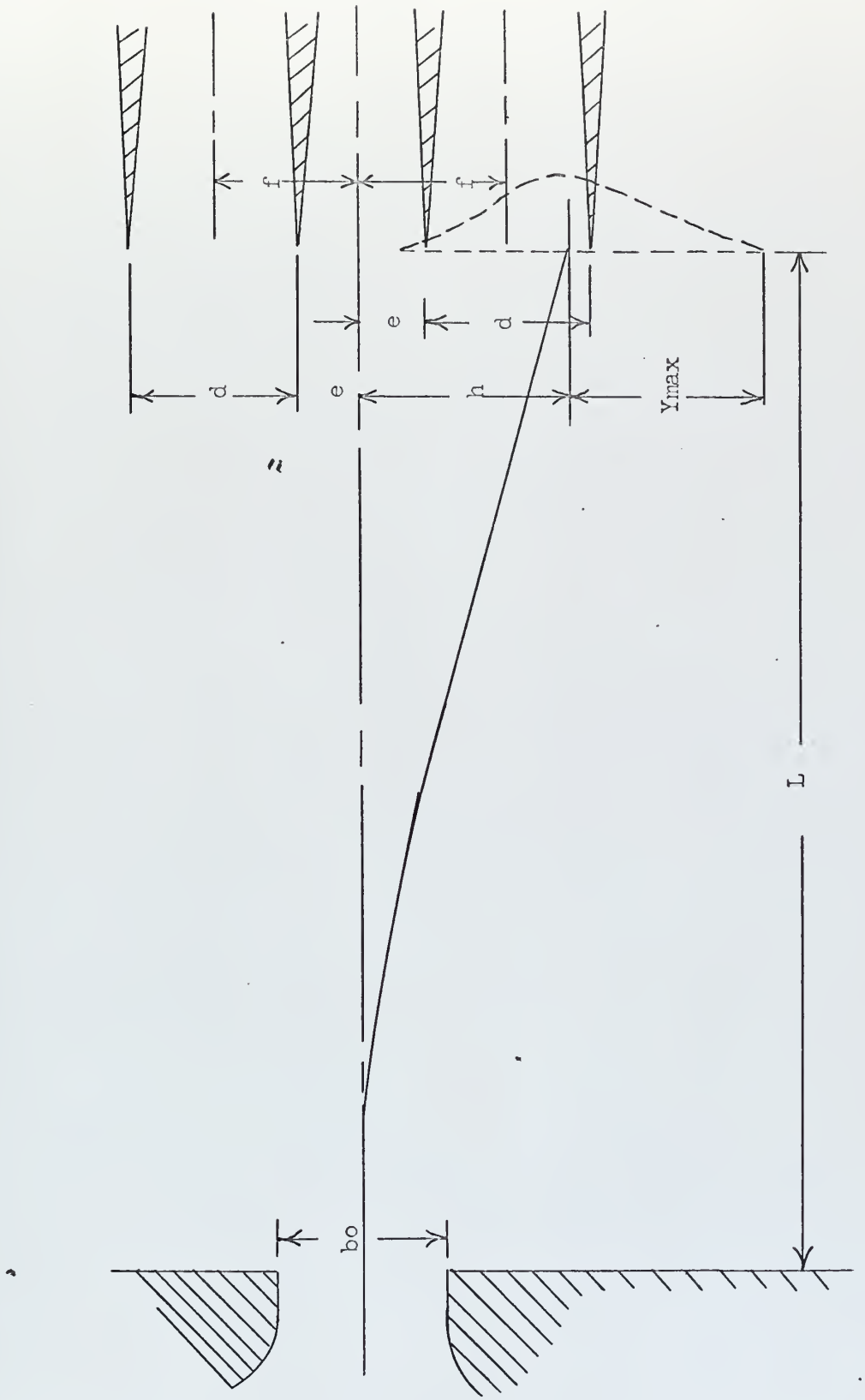

FIGURE 3 GEOMETRICAL RELATIONSHIPS OF THE RECEIVER PORTS

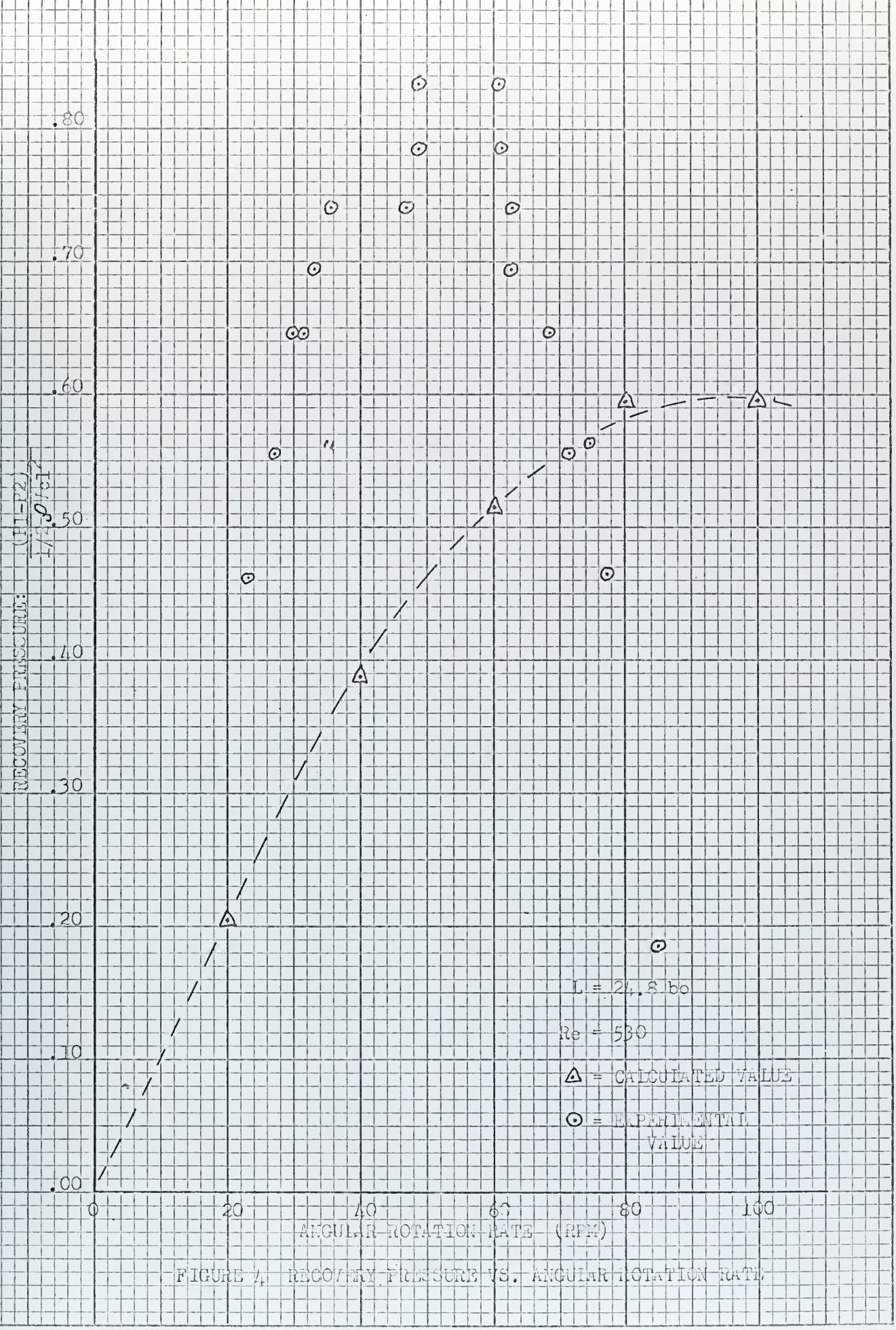

FIGURE 4. RECOVERY PRESSURE VS. ANGULAR ROTATION RATE

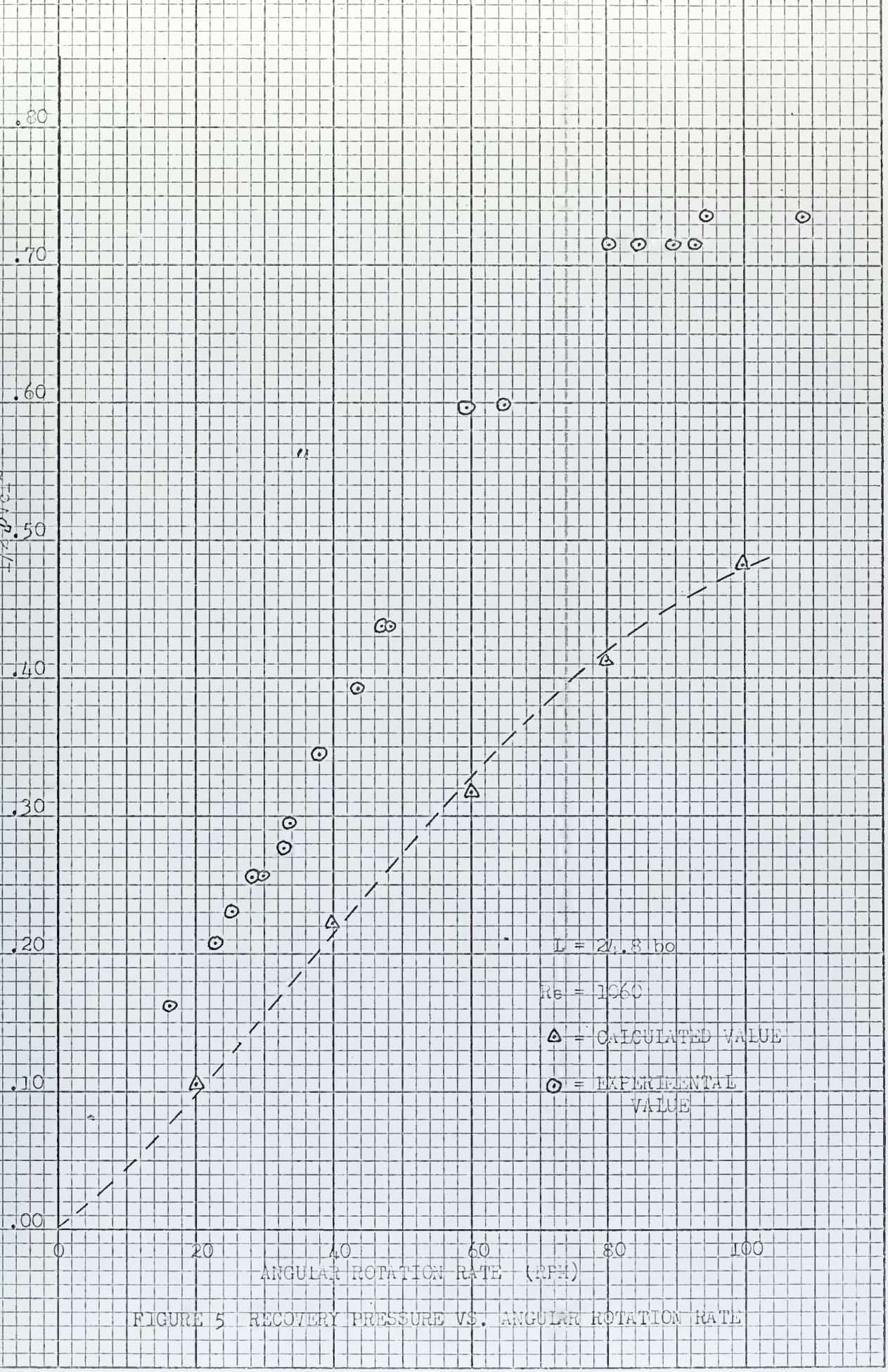

FIGURE 5 RECOVERY PRESSURE VS. ANGULAR ROTATION RATE

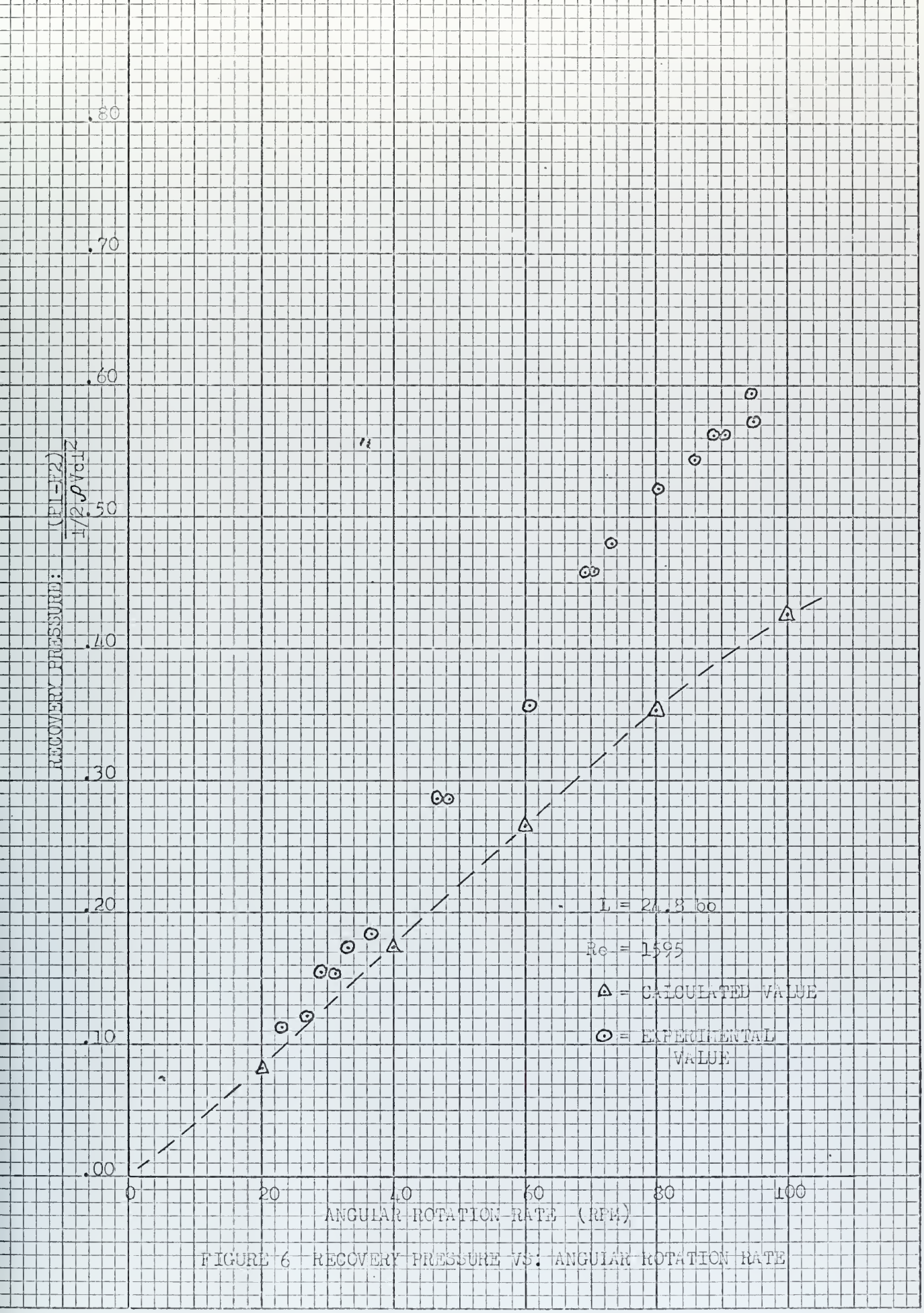

FIGURE 6 RECOVERY PRESSURE VS. ANGULAR ROTATION RATE

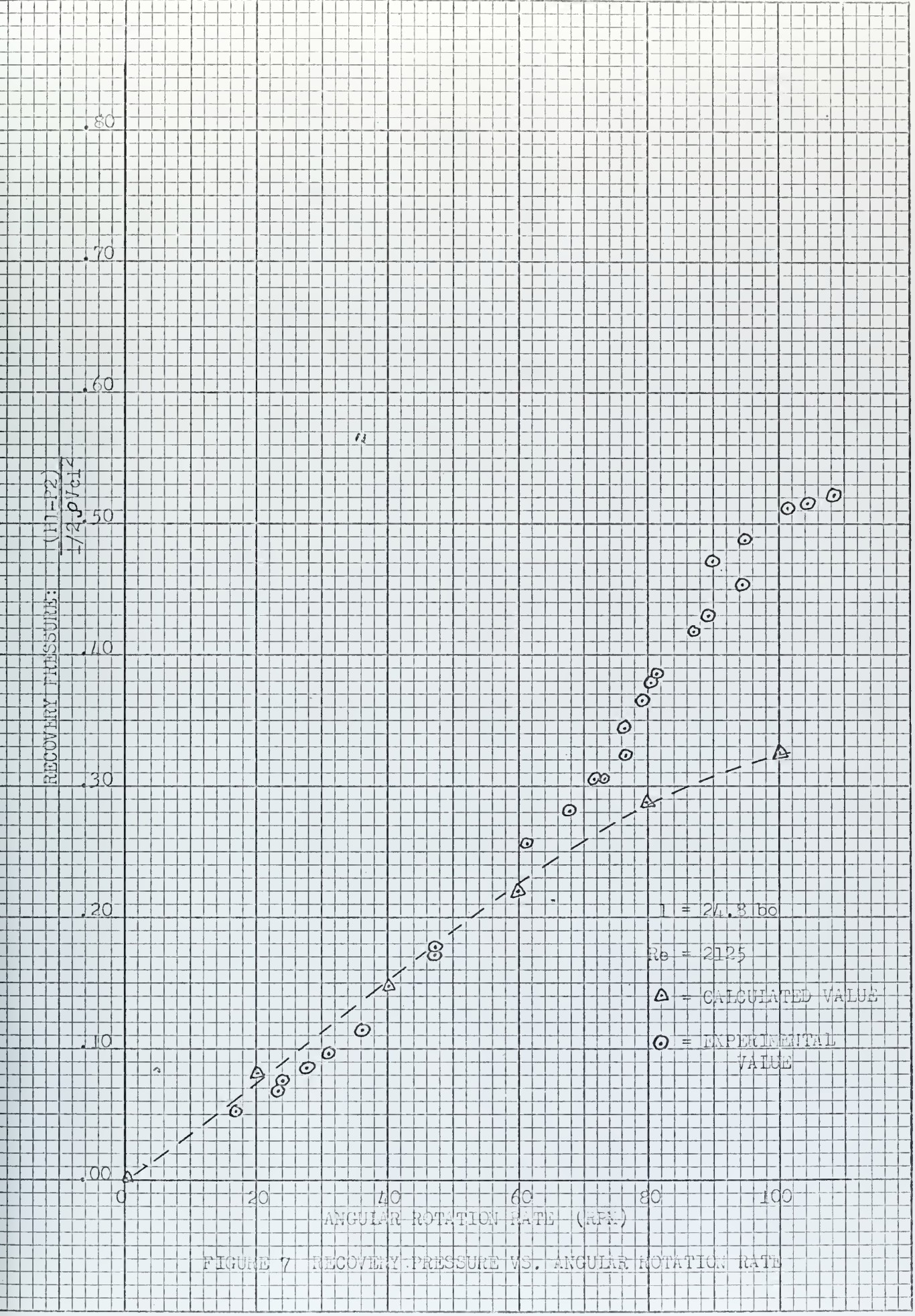

FIGURE 7 RECOVERY PRESSURE VS. ANGULAR ROTATION RATE

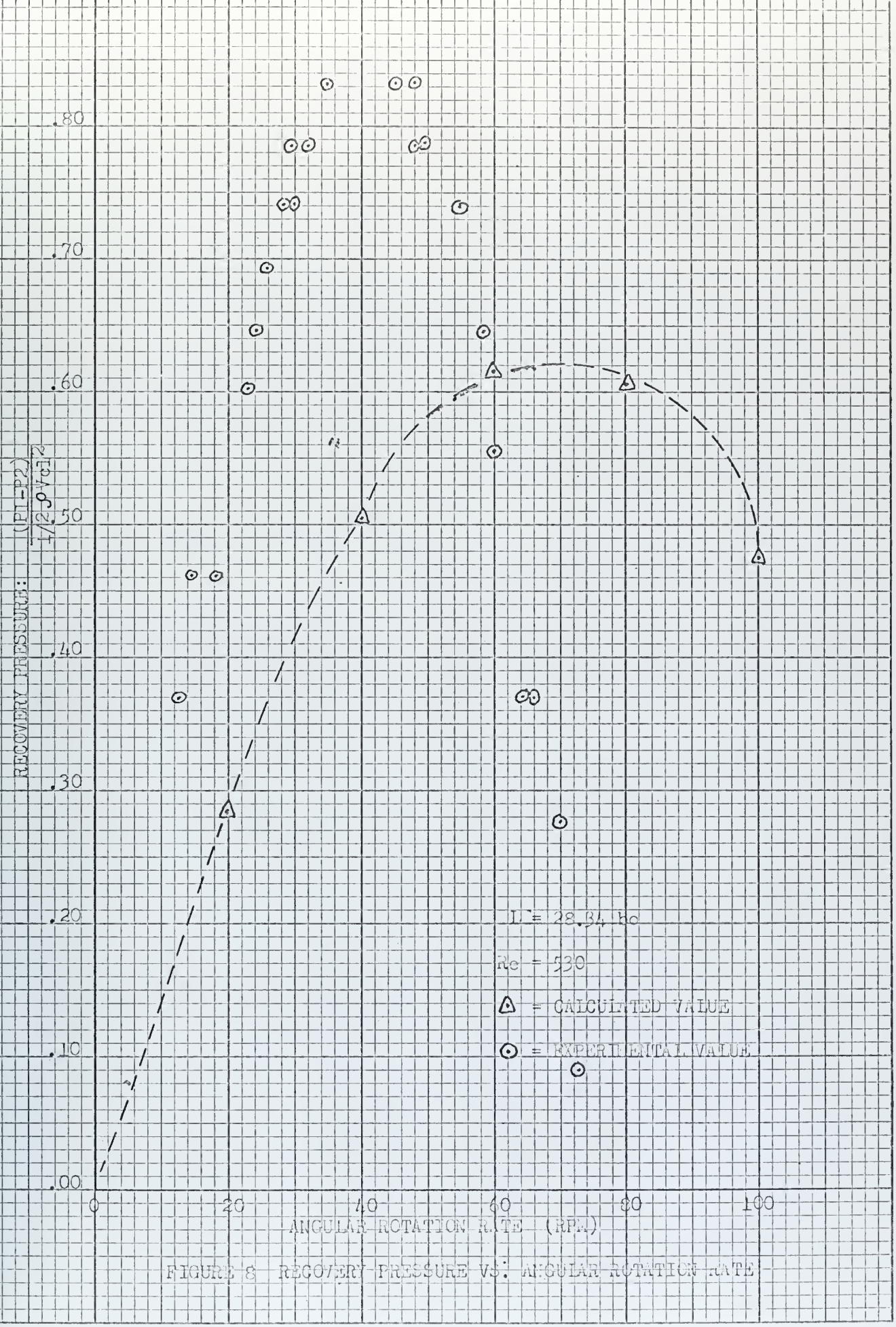

FIGURE 8 RECOVERY PRESSURE VS. ANGULAR ROTATION RATE

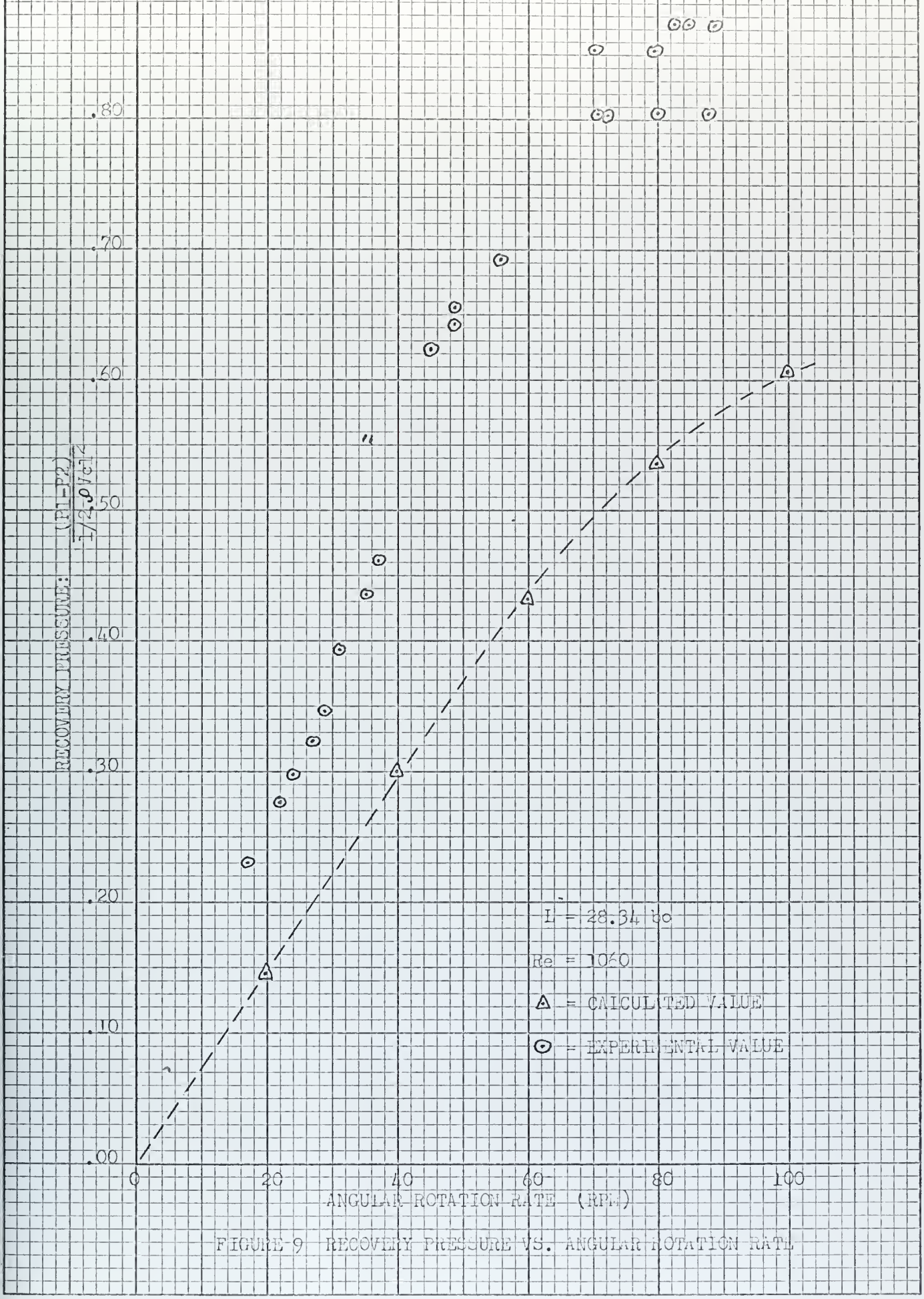

FIGURE 9 RECOVERY PRESSURE VS. ANGULAR ROTATION RATE

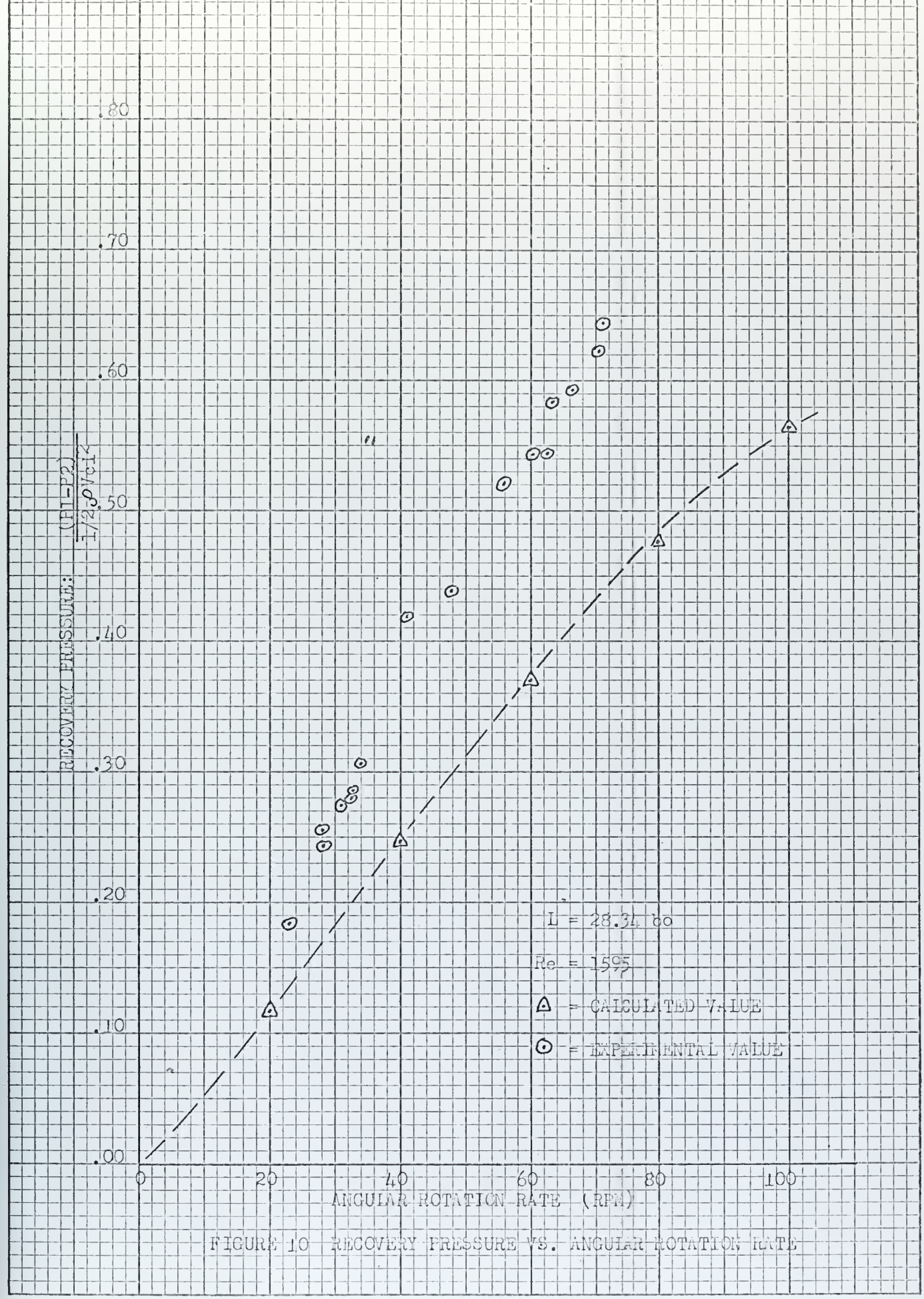

FIGURE 10 RECOVERY PRESSURE VS. ANGULAR ROTATION RATE

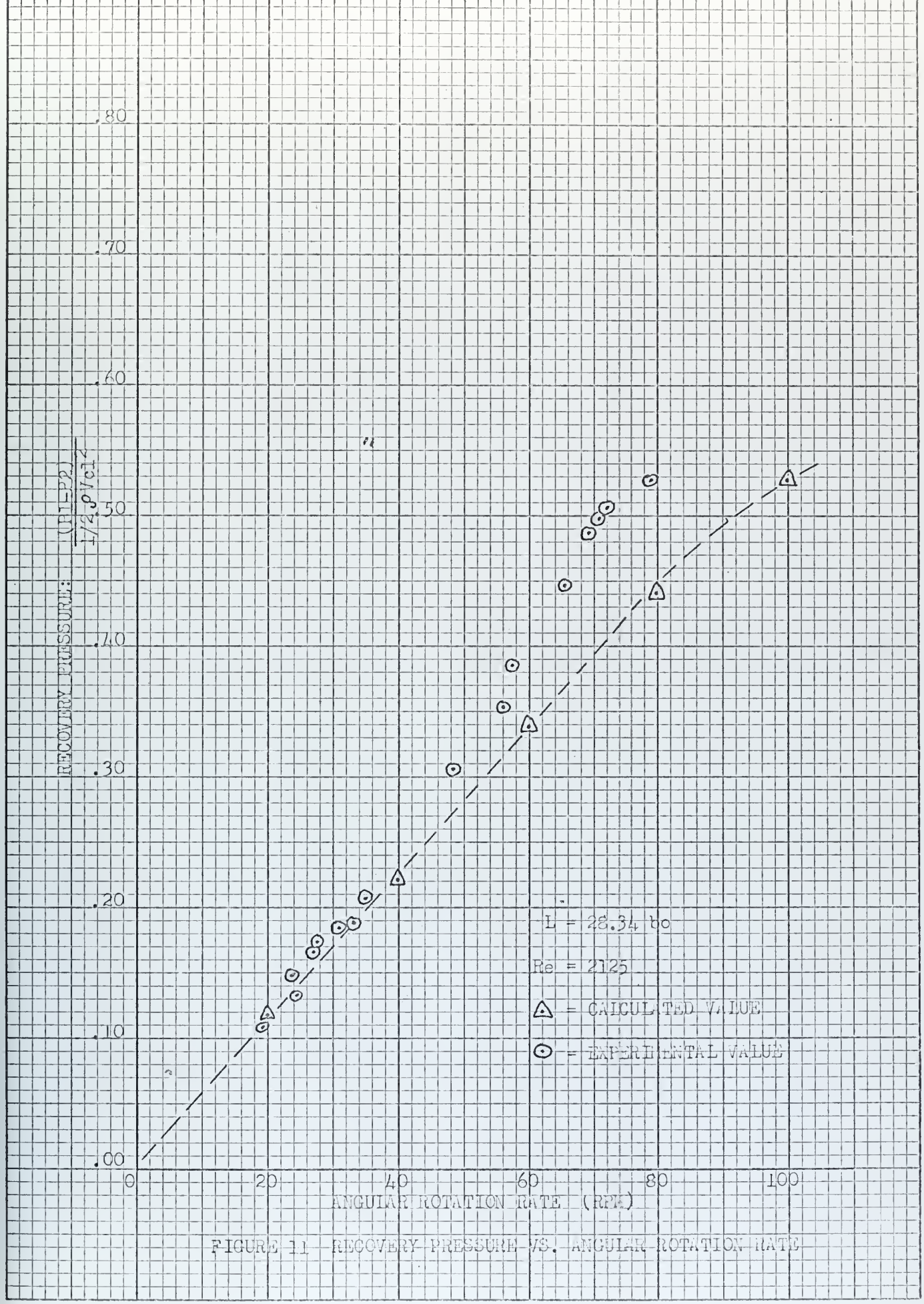

FIGURE 11 - RECOVERY PRESSURE VS. ANGULAR ROTATION RATE

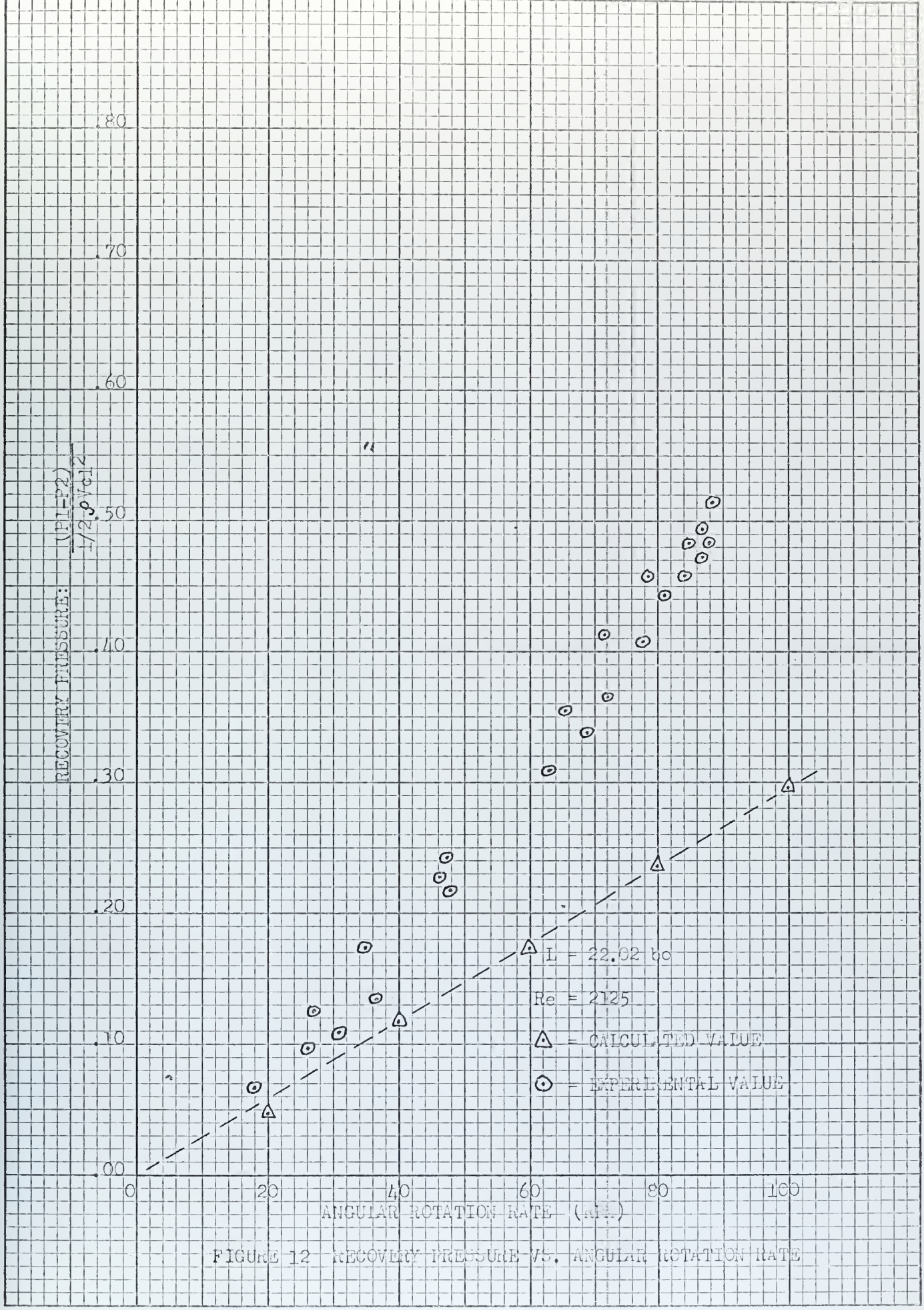

FIGURE 12 RECOVERY PRESSURE VS. ANGULAR ROTATION RATE

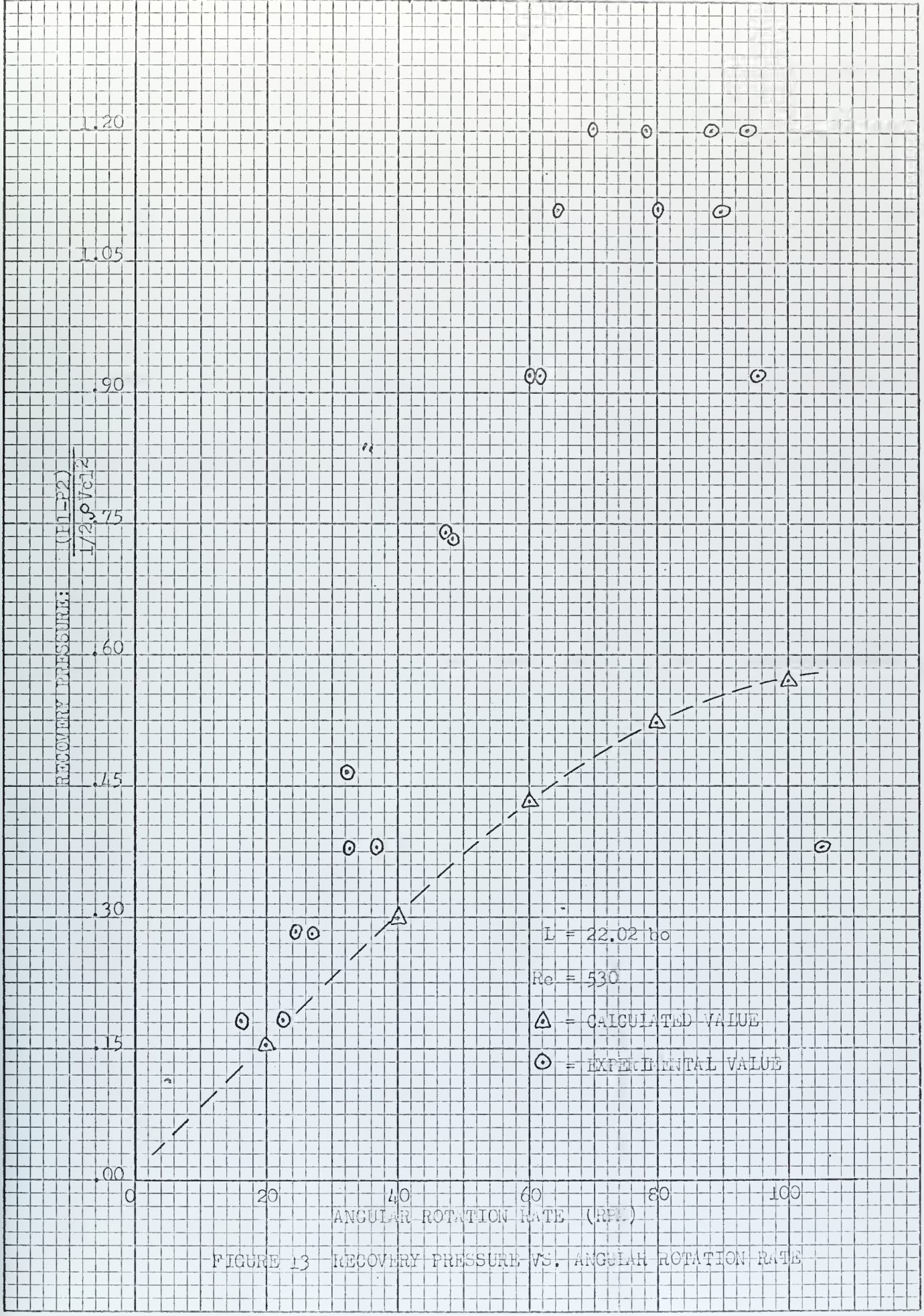

FIGURE 13 RECOVERY PRESSURE VS. ANGULAR ROTATION RATE

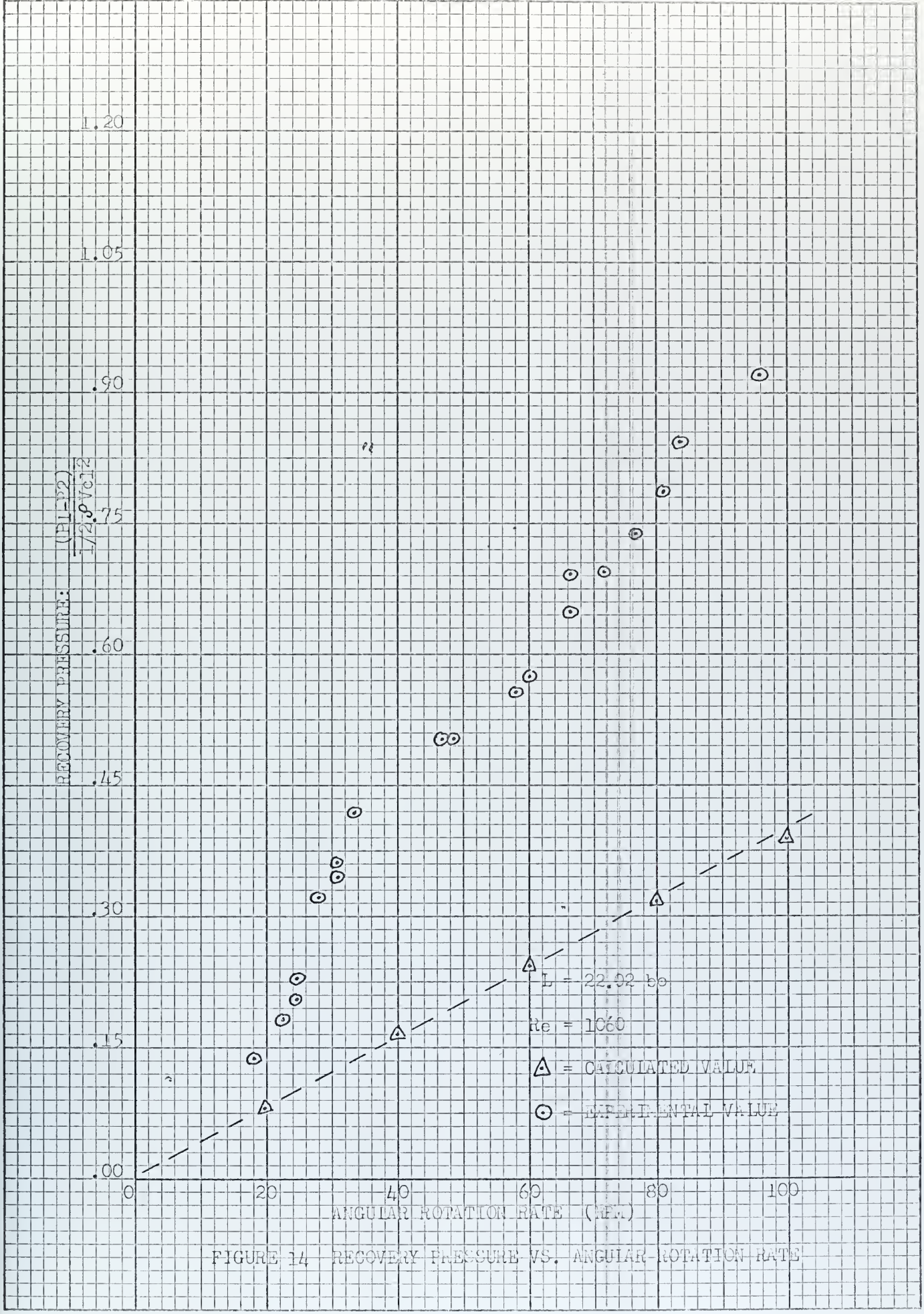

FIGURE 14 RECOVERY PRESSURE VS. ANGULAR ROTATION RATE

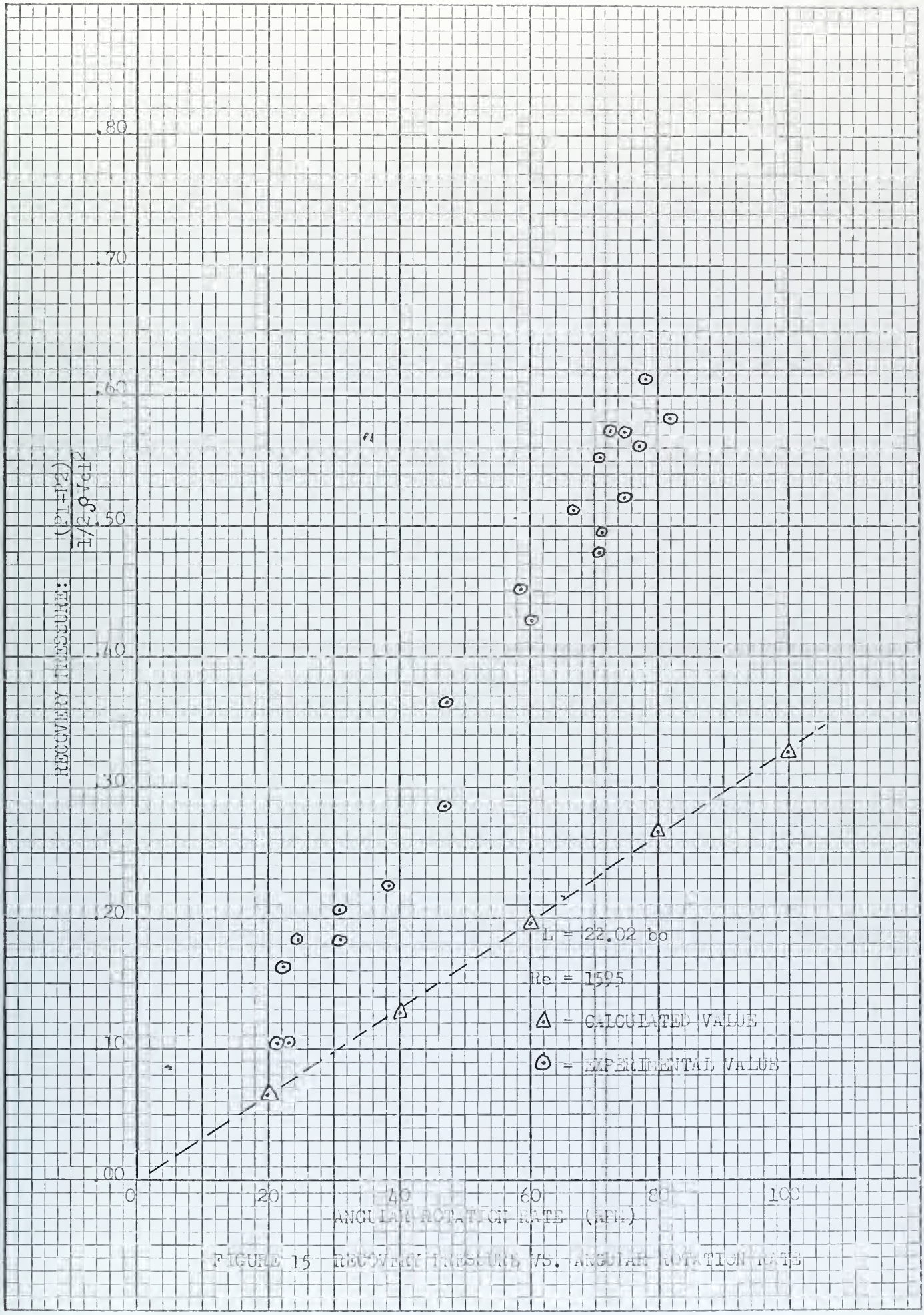

FIGURE 15 RECOVERY PRESSURE VS. ANGULAR ROTATION RATE

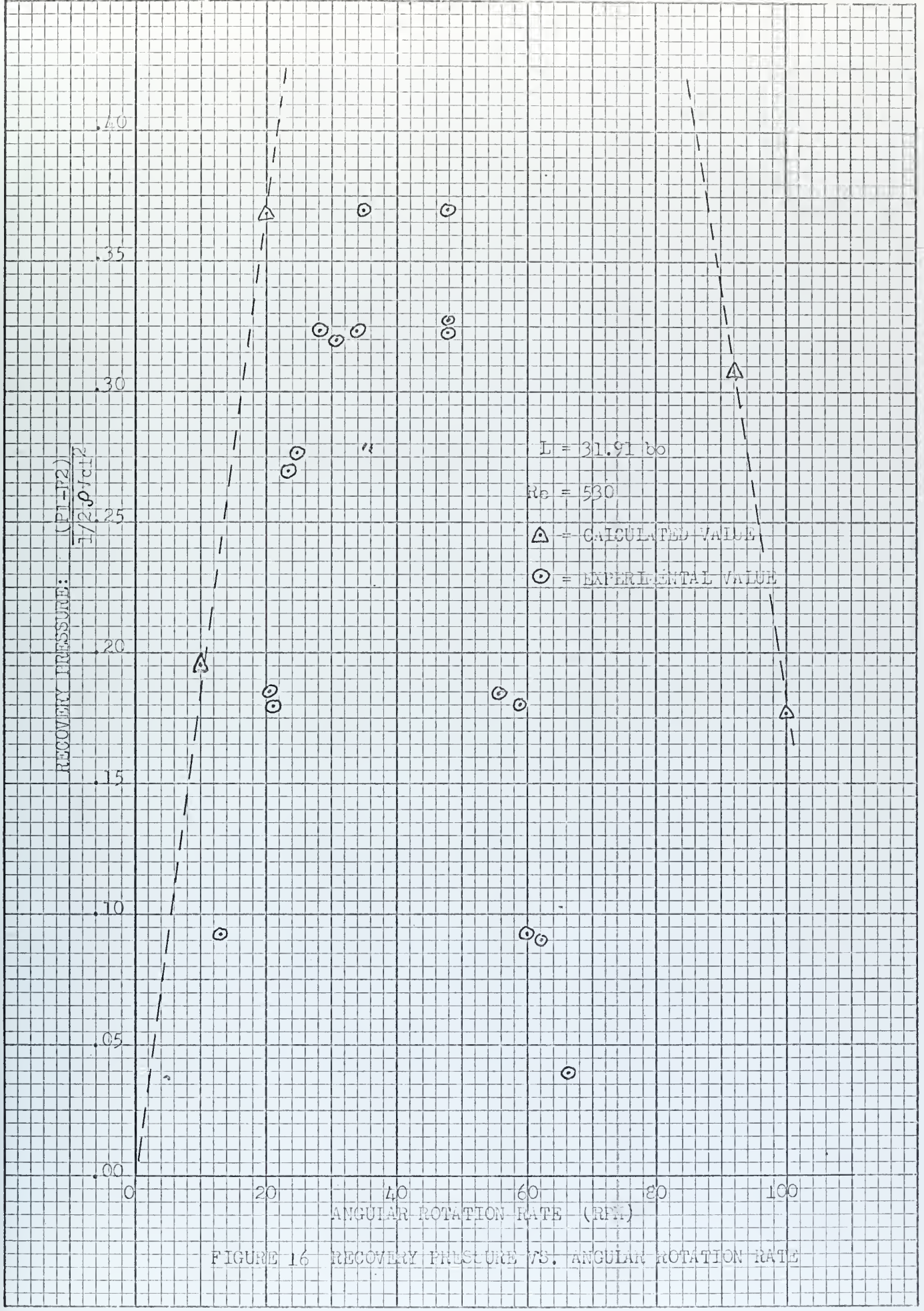

FIGURE 16 RECOVERY PRESSURE VS. ANGULAR ROTATION RATE

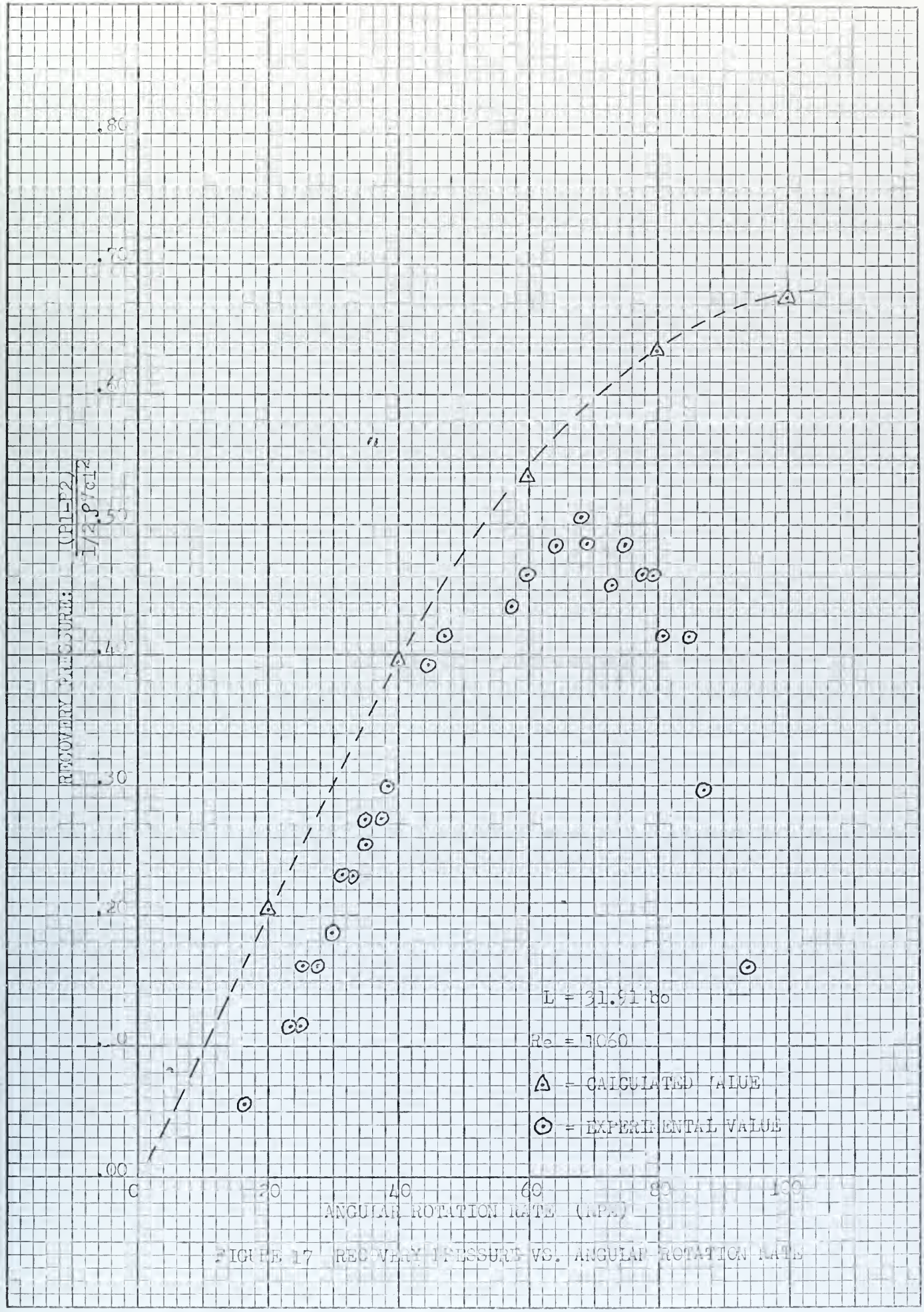

FIGURE 17 RECOVERY PRESSURE VS. ANGULAR ROTATION RATE

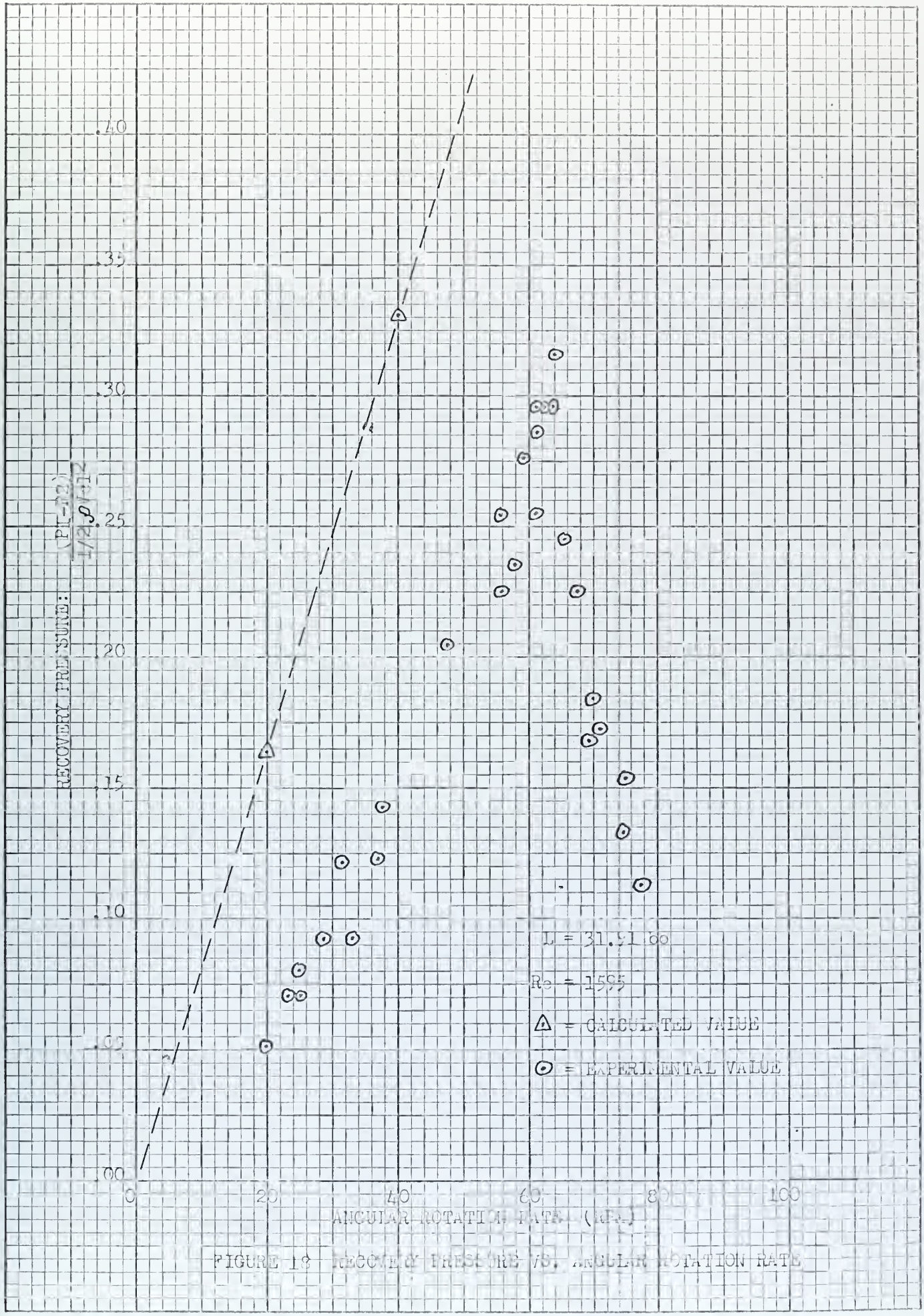

FIGURE 19 RECOVERY PRESSURE VS. ANGULAR ROTATION RATE

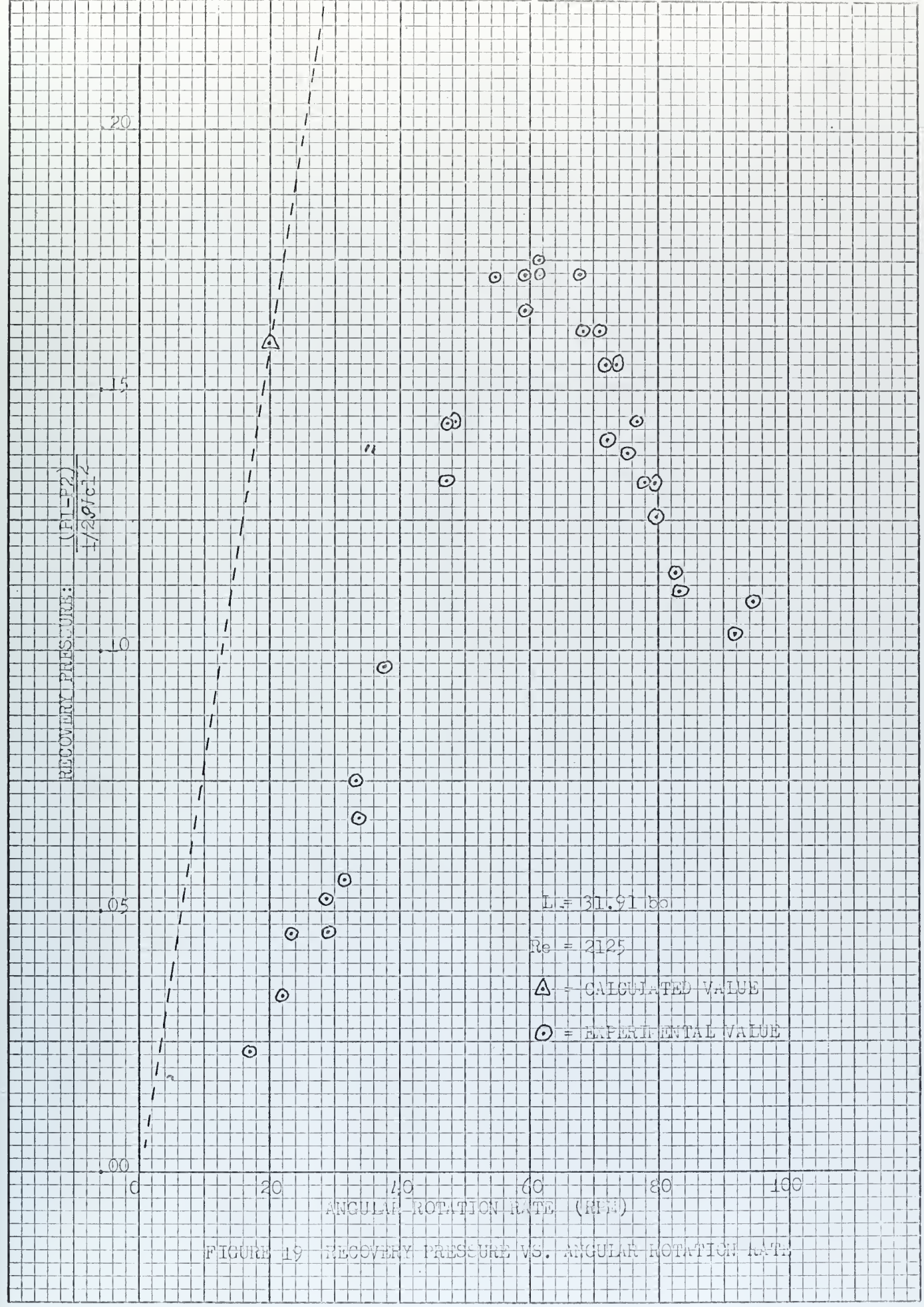

FIGURE 19 RECOVERY PRESSURE VS. ANGULAR ROTATION RATE

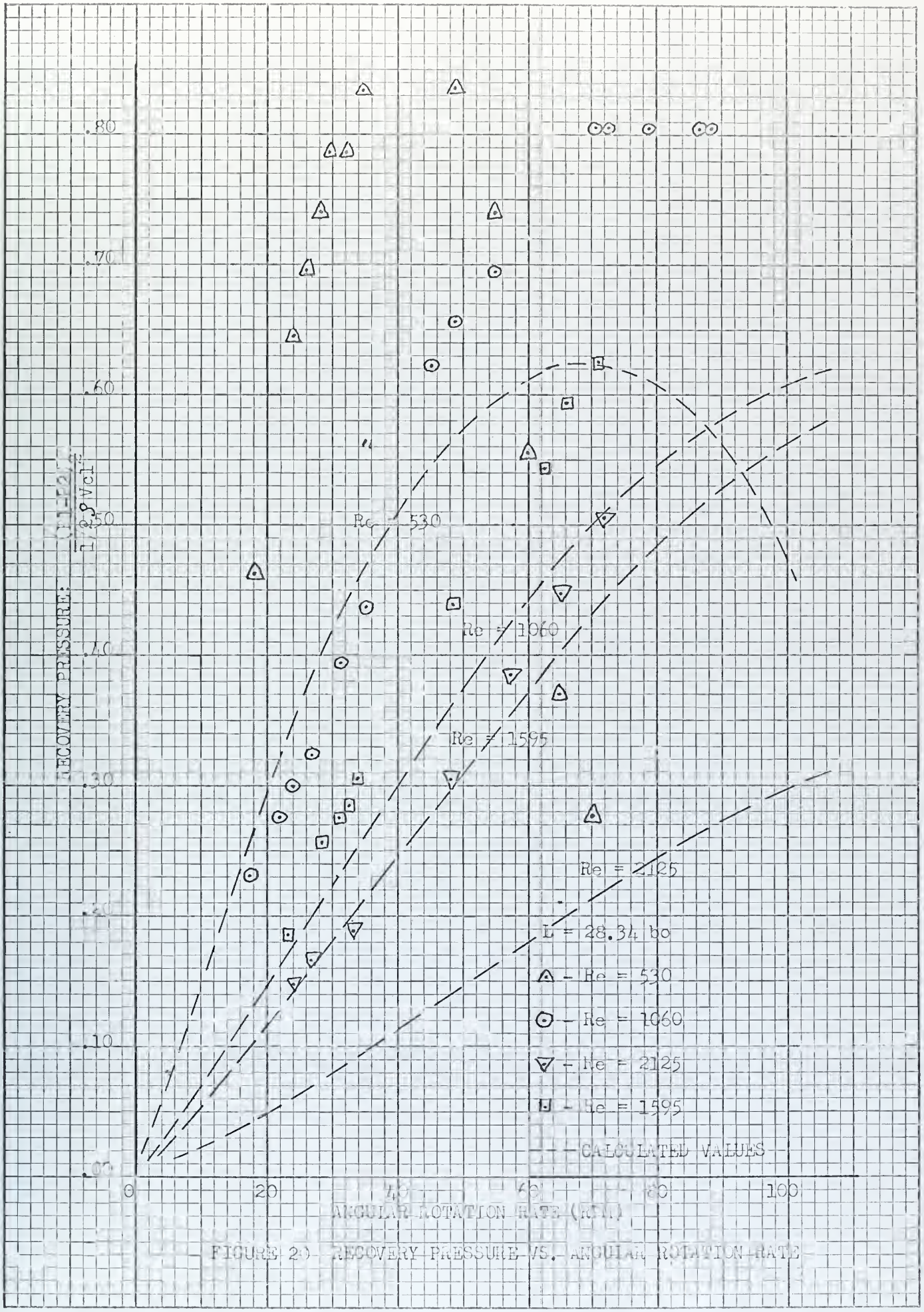

FIGURE 20 RECOVERY PRESSURE VS. ANGULAR ROTATION RATE

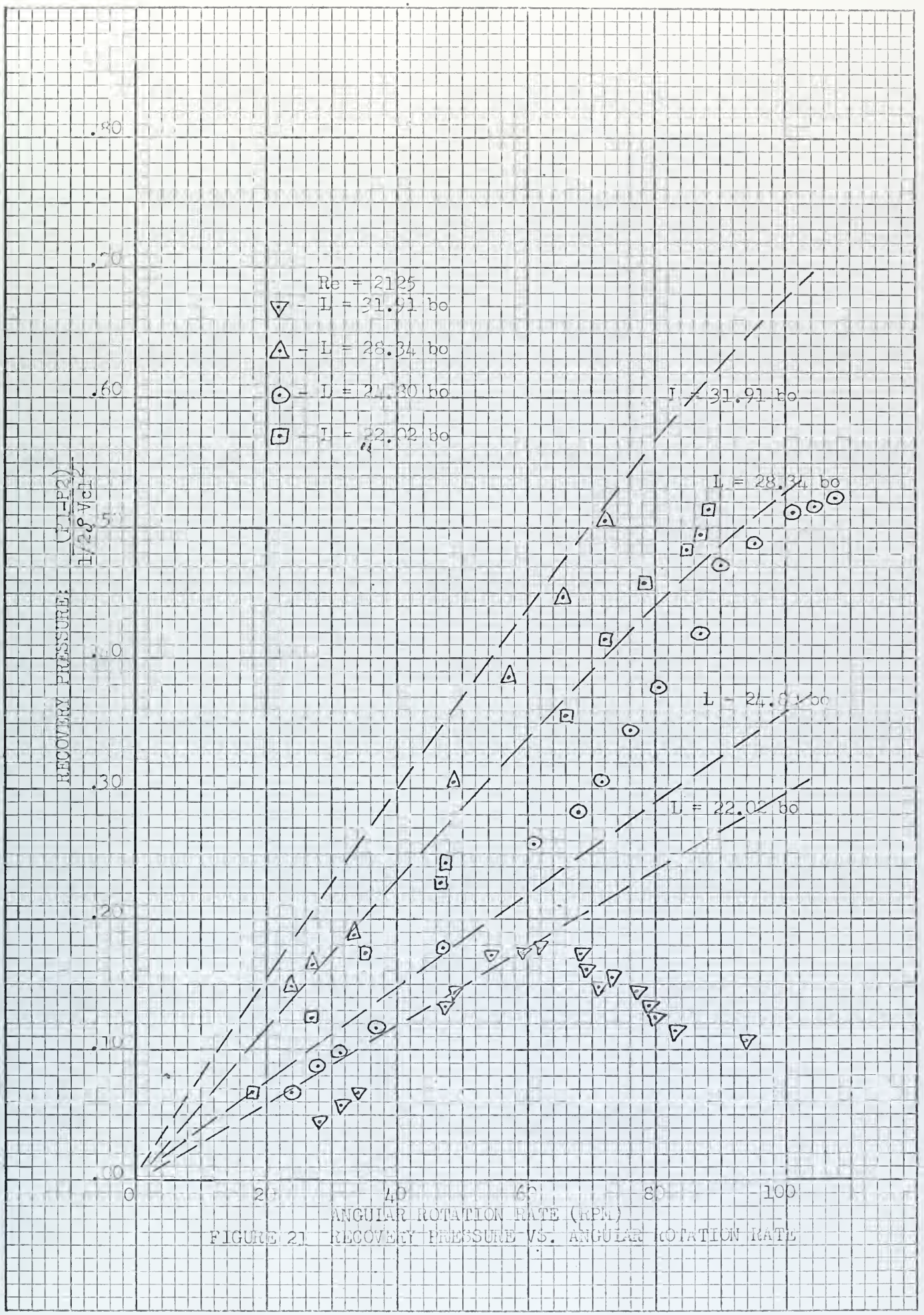

FIGURE 21 RECOVERY PRESSURE VS. ANGULAR ROTATION RATE

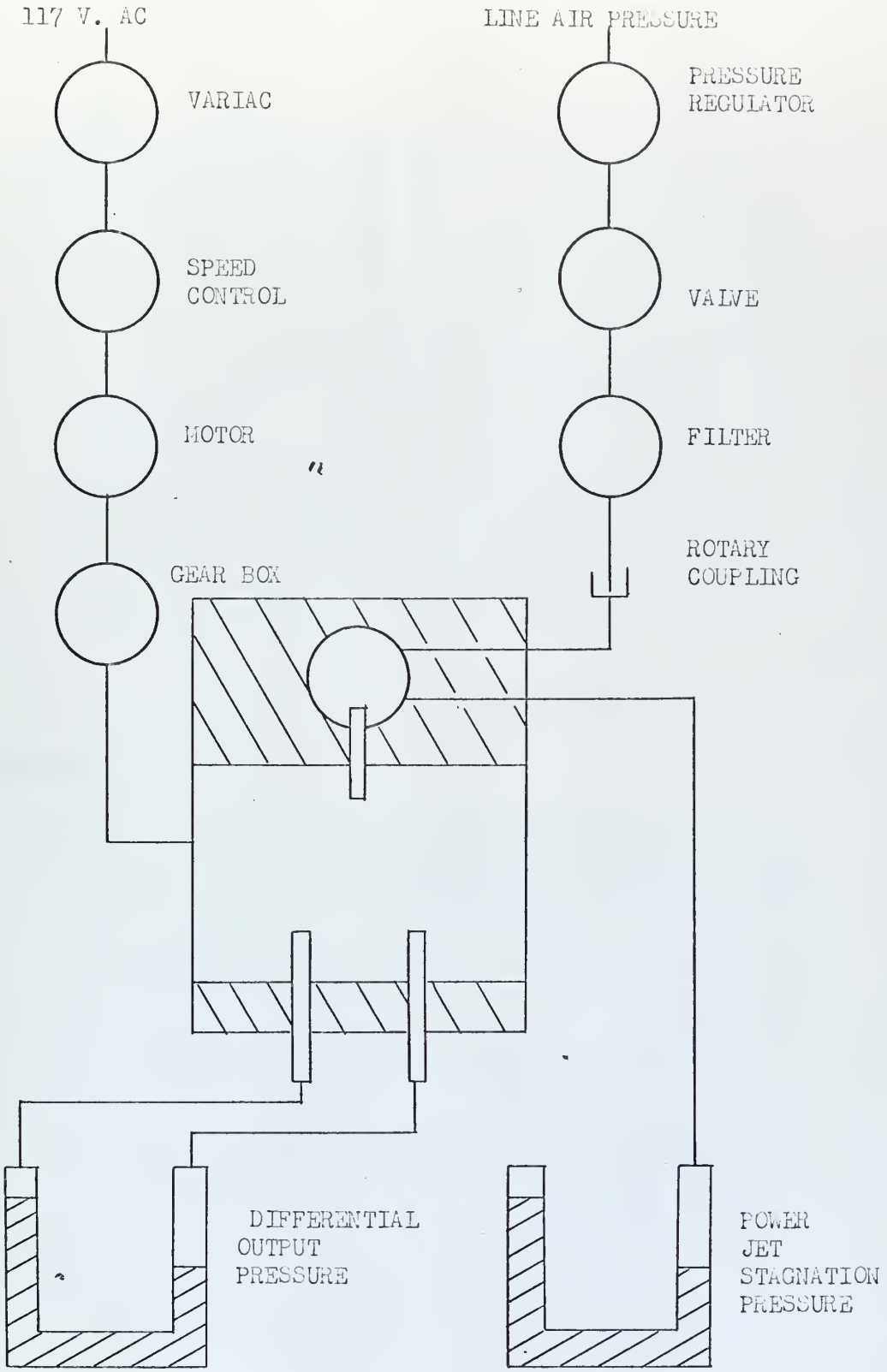

FIGURE 22 SCHEMATIC DRAWING OF THE EXPERIMENTAL APPARATUS

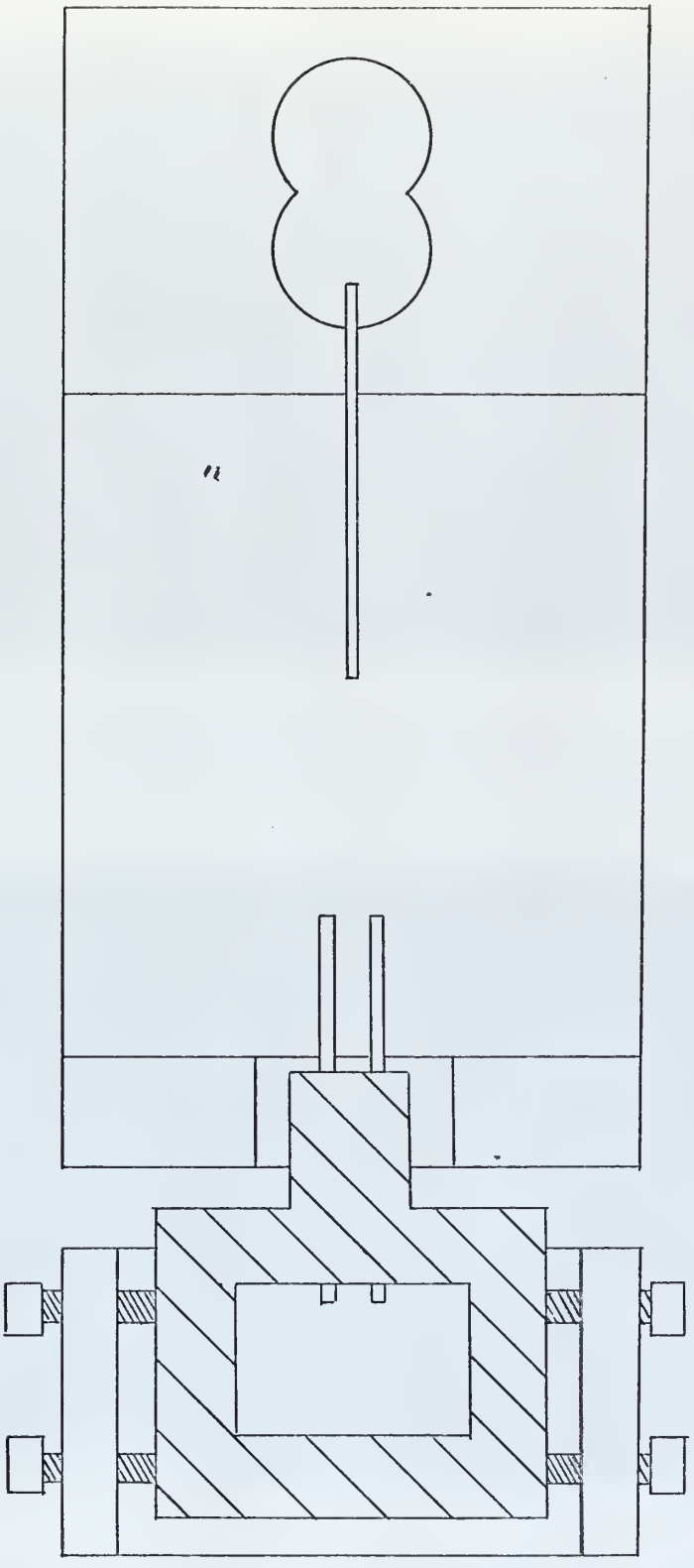

FIGURE 23 DETAIL DRAWING OF THE EXPERIMENTAL APPARATUS

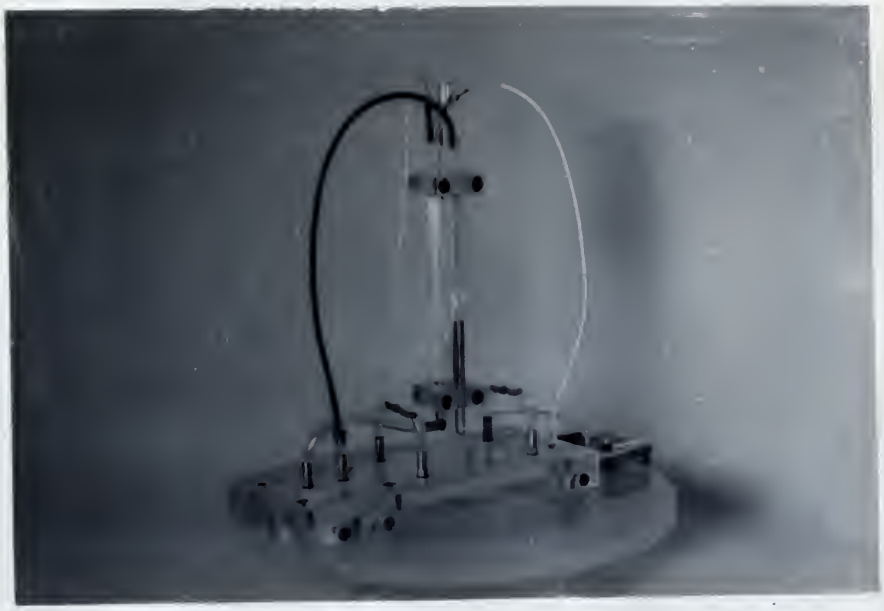

ASSEMBLED EXPERIMENTAL APPARATUS

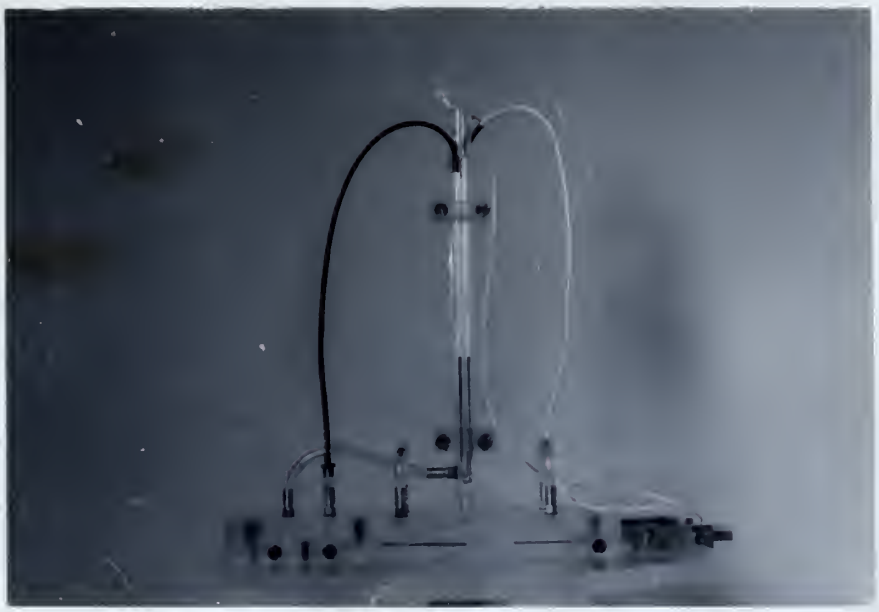

ASSEMBLED EXPERIMENTAL APPARATUS

FIGURE 24 PHOTOGRAPHS OF THE EXPERIMENTAL APPARATUS

COVER ASSEMBLY

COVER ASSEMBLY

FIGURE 25 PHOTOGRAPHS OF THE EXPERIMENTAL APPARATUS

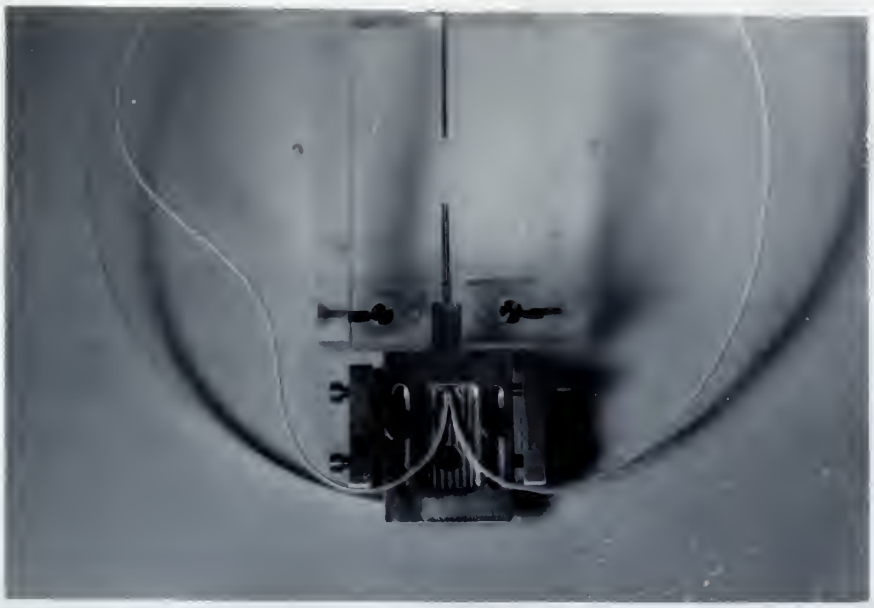

BASE ASSEMBLY

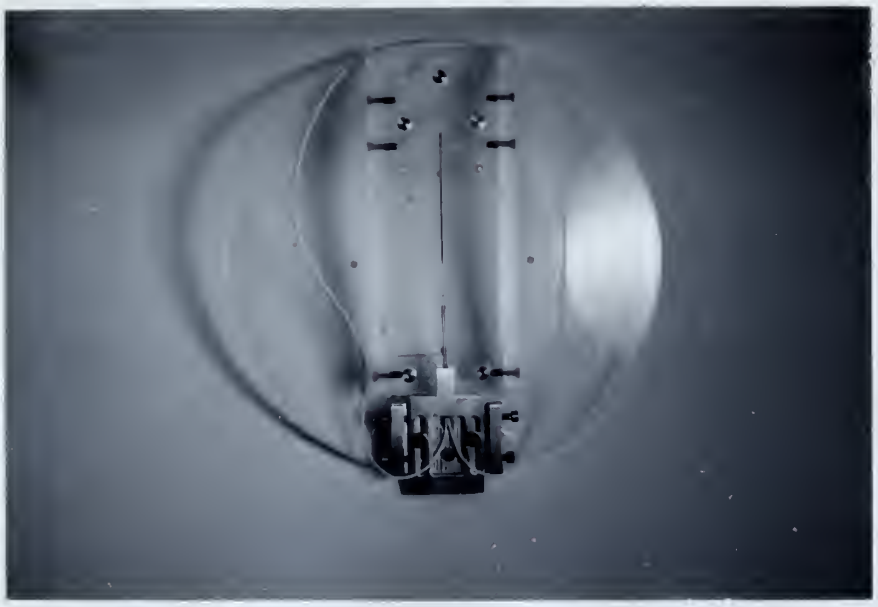

BASE ASSEMBLY

FIGURE 26 PHOTOGRAPHS OF THE EXPERIMENTAL APPARATUS

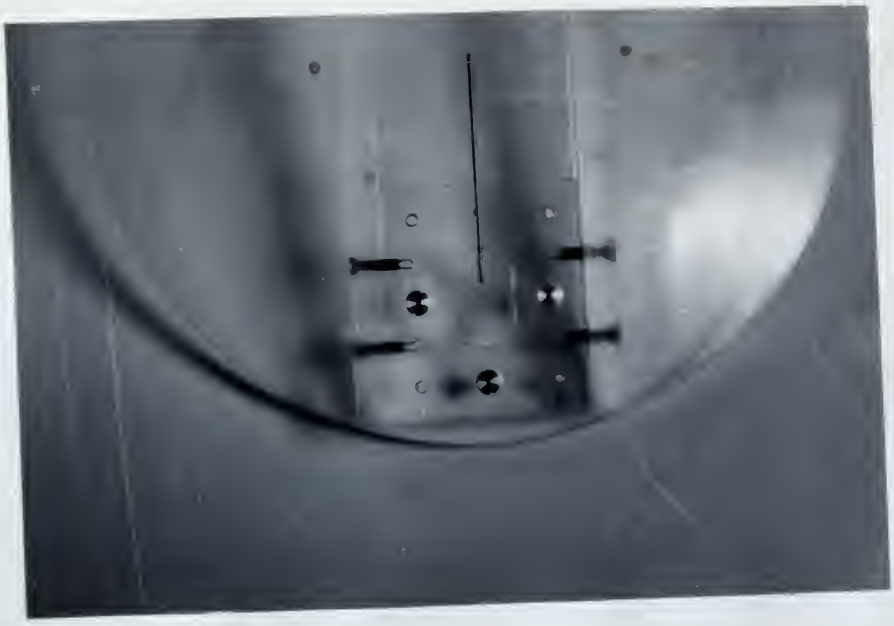

PLENUM CHAMBER

CARRIAGE ASSEMBLY

FIGURE 27 PHOTOGRAPHS OF THE EXPERIMENTAL APPARATUS

Thesis
P2657 Patterson 127271
Design and study of
a novel fluidic angular
rate sensing system
21 SEP 71
DISPLAY

Thesis
P2657 Patterson 127271
Design and study of
a novel fluidic angular
rate sensing system.

thesP2657
Design and study of a novel fluidic angu
3 2768 001 98065 9
DUDLEY KNOX LIBRARY